© 2020. Published by The Company of Biologists Ltd | Development (2020) 147, dev191544. doi:10.1242/dev.191544

STEM CELLS AND REGENERATION

RESEARCH ARTICLE

Dissecting Hes-centred transcriptional networks in neural stem cell maintenance and tumorigenesis in *Drosophila*

Srivathsa S. Magadi[1,2], Chrysanthi Voutyraki[1,2], Gerasimos Anagnostopoulos[1,2], Evanthia Zacharioudaki[1], Ioanna K. Poutakidou[1,2], Christina Efraimoglou[1,2], Margarita Stapountzi[1], Vasiliki Theodorou[1], Christoforos Nikolaou[1,2], Konstantinos A. Koumbanakis[1,2], John F. Fullard[1] and Christos Delidakis[1,2,*]

ABSTRACT

Neural stem cells divide during embryogenesis and juvenile life to generate the entire complement of neurons and glia in the nervous system of vertebrates and invertebrates. Studies of the mechanisms controlling the fine balance between neural stem cells and more differentiated progenitors have shown that, in every asymmetric cell division, progenitors send a Delta-Notch signal to their sibling stem cells. Here, we show that excessive activation of Notch or overexpression of its direct targets of the Hes family causes stem-cell hyperplasias in the *Drosophila* larval central nervous system, which can progress to malignant tumours after allografting to adult hosts. We combined transcriptomic data from these hyperplasias with chromatin occupancy data for Dpn, a Hes transcription factor, to identify genes regulated by Hes factors in this process. We show that the Notch/Hes axis represses a cohort of transcription factor genes. These are excluded from the stem cells and promote early differentiation steps, most likely by preventing the reversion of immature progenitors to a stem-cell fate. We describe the impact of two of these 'anti-stemness' factors, Zfh1 and Gcm, on Notch/Hes-triggered tumorigenesis.

KEY WORDS: *Drosophila*, Hes, Notch signalling, Cancer models in *Drosophila*, Neural stem cells, Transcription factors

INTRODUCTION

Drosophila neural stem cells (NSCs), also known as neuroblasts, are a well-studied system for stem cell self-renewal, differentiation and carcinogenesis. NSCs are born early in embryogenesis and, over the course of embryonic and juvenile (larval, early pupal) life, give birth to all neurons and glia that make up the central nervous system (Lee, 2017). They do so by undergoing asymmetric cell divisions that regenerate an NSC and also give rise to a more differentiated cell, usually a ganglion mother cell (GMC, Type I mode of division) or an intermediate neural precursor (INP, Type II) (Baumgardt et al., 2014; Homem et al., 2015). The GMC subsequently divides only once to give rise to two postmitotic cells (neurons or glia), whereas the INP can also self-renew, albeit for fewer rounds than an NSC, and generate GMCs. Similar asymmetric cell divisions have also been observed in vertebrate NSCs and the conservation extends beyond cellular phenomenology to the molecular players involved: many proteins that orchestrate fly NSC divisions have mammalian orthologues with similar functions (Paridaen and Huttner, 2014). This justifies the use of *Drosophila* to elucidate conserved features of neurogenesis and to pinpoint defects that can lead to runaway proliferation and potential malignant transformation of NSCs, which is the cause of many types of childhood and adult brain tumours.

One of the several consequences of the elaborate asymmetric cell division of the NSC is the unidirectional Delta-Notch signalling from the GMC/INP progeny to the NSC, achieved by asymmetrically segregating Numb, a Notch inhibitor, to the GMC (Knoblich et al., 1995; Spana and Doe, 1996). However, Notch signalling is not indispensable for NSC maintenance, as only minor defects are observed upon loss of Notch function: most Type I lineages are unaffected, whereas Type IIs terminate prematurely (Almeida and Bray, 2005; Wang et al., 2006; Zacharioudaki et al., 2012). Transcription factors (TFs) of the Hes family are common Notch targets across tissues and species. During *Drosophila* neurogenesis, the NSCs express *dpn* and at least three E(spl) genes out of the 11 Hes genes in the fly genome (Almeida and Bray, 2005; Bier et al., 1992; Zacharioudaki et al., 2012; see also Fig. S1). Double knockout of *dpn* and the E(spl) complex results in acute NSC loss by premature termination of both Type I and Type II lineages (Zacharioudaki et al., 2012; Zhu et al., 2012). Even though E(spl) genes as well as *dpn* are induced by Notch (Almeida and Bray, 2005; San-Juán and Baonza, 2011), we showed that Dpn expression persists in *Notch* loss-of-function (Zacharioudaki et al., 2012), justifying the weaker *Notch* phenotype. Therefore, the Hes TFs and, to a lesser extent, Notch are central to the maintenance of stemness in fly NSCs. The dependence of NSC maintenance on Hes activity and Notch has also been documented in mammals (Kageyama et al., 2019).

Unlike the mild loss-of-function effects of Notch, its overactivation has dramatic consequences on neurogenesis: many immature differentiating cells revert to NSCs, causing extensive NSC hyperplasia at the expense of differentiated neuronal progeny in the larval CNS (Bowman et al., 2008; Wang et al., 2006; Weng et al., 2010; Zacharioudaki et al., 2012). This effect is complete in Type II lineages, but it is also evident in Type Is, albeit with reduced penetrance. Overexpression of *dpn* or *E(spl)mγ* (*E(spl)mγ-HLH*) did not disturb Type I lineages and gave only mild hyperplasias in Type II lineages (Zacharioudaki et al., 2016, 2012). Other genetic insults can give rise to NSC hyperplasia in larval CNSs, typified by *brat* or *pros* loss-of-function (Kang and Reichert, 2015). Both of these gene products are asymmetrically segregated in the GMC and/or INP (only Brat in the latter, as *pros* is not expressed in Type II NSCs) and function to regulate transcription (Pros) or translation (Brat) (Choksi et al., 2006; Loedige et al., 2015; Reichardt et al., 2018). Compromising the function of the asymmetric cell division machinery [e.g. mutations in *insc*, *pins*, *l(2)gl*, *dlg1*] also often leads to NSC hyperplasia (Caussinus

[1]Institute of Molecular Biology & Biotechnology, Foundation for Research & Technology Hellas, 70013 Heraklion, Crete, Greece. [2]Department of Biology, University of Crete, 70013 Heraklion, Crete, Greece.

*Author for correspondence (delidaki@imbb.forth.gr)

S.S.M., 0000-0002-7926-5970; C.V., 0000-0003-0943-0384; V.T., 0000-0003-1614-700X; C.N., 0000-0003-3001-6786; J.F.F., 0000-0001-9874-2907; C.D., 0000-0003-3912-701X

Handling Editor: François Guillemot
Received 16 April 2020; Accepted 5 October 2020

Development (2020) 147, dev191544. doi:10.1242/dev.191544

and Gonzalez, 2005; Gateff, 1978). These hyperplasias are prone to malignant overgrowth and metastasis to distant sites upon allografting to an adult host. It was not known whether the Notch-dependent hyperplasias also have a malignant potential.

Here, we revisited the ability of Hes TFs to cause NSC hyperplasia and tested the ability of both Notch and Hes induced hyperplasias to progress to malignant tumours. We show that, upon ectopically expressing pairs of Hes transgenes, we can elicit severe NSC hyperplasias. These hyperplasias, as well as those caused by Notch overactivation, are malignant upon allografting. Comparison of hyperplastic CNS transcriptomes showed high similarity between two different combinations and moderate similarity between these and the high-Notch hyperplasias. Much less similarity was found with other known NSC tumour transcriptomes deposited in databases, pointing to a Hes/Notch-type of tumour. As Hes proteins are known to act as repressors, we focussed on the downregulated targets which are, at the same time, bound by Dpn, shown using chromatin immunoprecipitation (ChIP). These were enriched for TFs, among which were *pros* and *nerfin-1*, known to prevent GMCs and early neurons from reverting to an NSC fate, as well as *erm* which does the same in Type II INPs. We chose to study two other Hes-downregulated TFs, Zfh1 and Gcm, in more detail, and will present their expression patterns and possible roles in modulating tumorigenesis.

RESULTS

Overexpression of Hes genes causes malignant NSC tumours

Overexpression of activated Notch has been known to cause NSC hyperplasia in larvae (Wang et al., 2006) and our earlier work (Zacharioudaki et al., 2016, 2012) has shown that this is accompanied by induction of Hes genes *dpn* and *E(spl)mγ* and is suppressed by deletion of the E(spl) locus. We have also shown that the mild Type II hyperplasias caused by *E(spl)mγ* overexpression bypass the need for Notch activation. To test whether stronger defects can be observed by Hes gene overexpression we increased the transgene dose by expressing two copies of Hes genes. We selected to co-express either *E(spl)mγ+E(spl)m8* or *E(spl)mγ+dpn*, as these are normally expressed in larval NSCs (Fig. S1) and we have previously shown that these combinations give strong DNA binding as heterodimers *in vitro* (Koumbanakis, 2007; Zacharioudaki et al., 2012). Both global NSC-lineage overexpression by *grhNB-Gal4* and clonal overexpression by *act>STOP>Gal4* were performed. We imaged control and hyperplastic CNSs using NSC markers Dpn and Mira, NSC/GMC markers Ase and Wor, GMC/neuron marker Pros (nuclear), neuron marker Elav and glia marker Repo. Using the *grhNB-Gal4* driver (Fig. S2), we observed a large number of ectopic NSCs, not only at their normal superficial location but also invading deeper cortical layers, normally occupied by neurons (Fig. 1A-F). At the same time there was a deficit in Elav-positive neurons throughout the central brain and thoracic ganglion, regions in which *grhNB-Gal4* is expressed. Overexpression of Hes genes was less disruptive than overexpression of *NΔecd*, an activated form of Notch lacking its extracellular domain: *E(spl)mγ+dpn*-overexpressing animals survived to pupation, although they almost never made it to adulthood; in comparison, *NΔecd* animals died as early larvae unless *grhNB-Gal4* was kept inactive using a Gal80ts inhibitor until the last day of larval life.

Using random clonal expression *(hs-FLP*; *act>STOP>Gal4*) we could focus on the response of individual lineages. We shall henceforth use a shorthand notation for the three effector genotypes: *N* for *UAS-NΔecd*, *MM* for *UAS-E(spl)mγ+UAS-E(spl)m8* and *DM* for *UAS-dpn+UAS-E(spl)mγ*. In these FLP-out clones, Type II lineages were severely affected (Fig. S3), exhibiting a massive size increase with almost complete absence of differentiating cells (Pros-, Elav- or Repo-positive); only a small number of escapers turned on Pros or Elav, and these escapers were more frequent in *DM* and *MM* than in *N* clones. In *N* clones almost all cells expressed the NSC marker Dpn; in *MM* there were many Dpn-positive cells, but also many Dpn/Pros-double negative cells. In *DM* clones all cells were Dpn-positive by design (*UAS-dpn* overexpression), although its levels varied greatly from cell to cell, pointing to post-translational regulation of Dpn protein. Unlike Type II lineages, Type Is showed NSC hyperplasia with variable penetrance and expressivity (Fig. 1G-K). About 30% looked like the wild type (wt), whereas 70% contained three or more (up to 176) Dpn-positive NSC-like cells; all clones contained differentiating cells (Pros/Elav-positive). Phenotype expressivity (number of Dpn-positive cells per lineage) was higher in *N* than in *MM* clones. As in Type II, *DM* clones expressed Dpn broadly, albeit at variable levels from cell to cell within the same clone. The ectopic NSC-like cells were dispersed and were sometimes located in deep cortical layers, away from the parent NSC, where postmitotic neurons normally reside. Elav and Pros were partially repressed. Elav repression was more effective in *N* than in *MM* or *DM*. As a rule, cells that accumulated high levels of Dpn downregulated Elav, although in *MM* clones Dpn-negative/Elav-negative cells were often seen. Nuclear Pros downregulation was less common, in fact many cells were found to co-express Dpn and nuclear Pros in *N* clones (but not in *MM*), suggesting that *N* misexpression turns on Dpn before turning off Pros (Fig. S4). These phenotypes are consistent with a scenario in which ectopic Notch or Hes activity causes dedifferentiation of some GMCs (adjacent to the NSC) and early neurons (in deeper layers) back to an NSC-like fate (Fig. 1L). Using combinations of two UAS transgenes to equalize the dosage, we found the phenotypic severity in Type I lineages to be *N>DM>MM=2xmγ>2xdpn* (Fig. S5). Some of the dedifferentiated clones contain NSCs as late as in pupal or even adult stages (Fig. S6), a time when normal NSCs have ceased proliferating and are not detectable anymore (Homem et al., 2015; Lee, 2017; Maurange et al., 2008; Sousa-Nunes et al., 2010). Contrary to the behaviour of NSC lineages, misexpression of *N*, *MM* or *DM* in post-mitotic mature neurons (single-cell clones located in deep layers, close to the neuropils or in the abdominal ganglion) did not result in loss of Elav (Fig. 1H-J, blue arrows), suggesting that Notch/Hes activity is effective in causing dedifferentiation only within a certain competence window after neuron birth.

To determine whether the NSC hyperplasias produced by persistent Notch/Hes activity are malignant we used an allograft assay (Rossi and Gonzalez, 2015). In *Drosophila*, a tissue is characterized malignant if it can overgrow upon transplantation to an adult host to the point of causing its premature death. We transplanted brain lobes or ventral nerve cords (VNCs) containing *act>STOP>Gal4* FLP-out clones driving *N*, *MM* or *DM* into young adult female abdomens. Out of the flies that survived the transplantation process, 33-98% developed tumours, seen as increased GFP fluorescence throughout the body, away from the transplantation site; these flies had a significantly lower survival rate than siblings allografted with wt tissue (Fig. 2A,B). Tumour tissue dissected out of the body cavity of host flies was retransplanted into new hosts, whereupon tumour growth was observed in ∼100% of injected hosts, and this could be repeated for many rounds (E.Z., C.V., V.T., I.K.P., C.E., S.S.M. and C.D., unpublished). Therefore, persistent Hes expression or excessive Notch signalling are sufficient to cause malignant transformation to larval NSC lineages. The fact that we readily recovered transplantable tumours even from VNC allografts suggests that Notch and Hes can drive malignancies not only from Type II, but also from Type I lineages (Fig. 2A). Histological examination of tumours 10-20 days

Development (2020) 147, dev191544. doi:10.1242/dev.191544

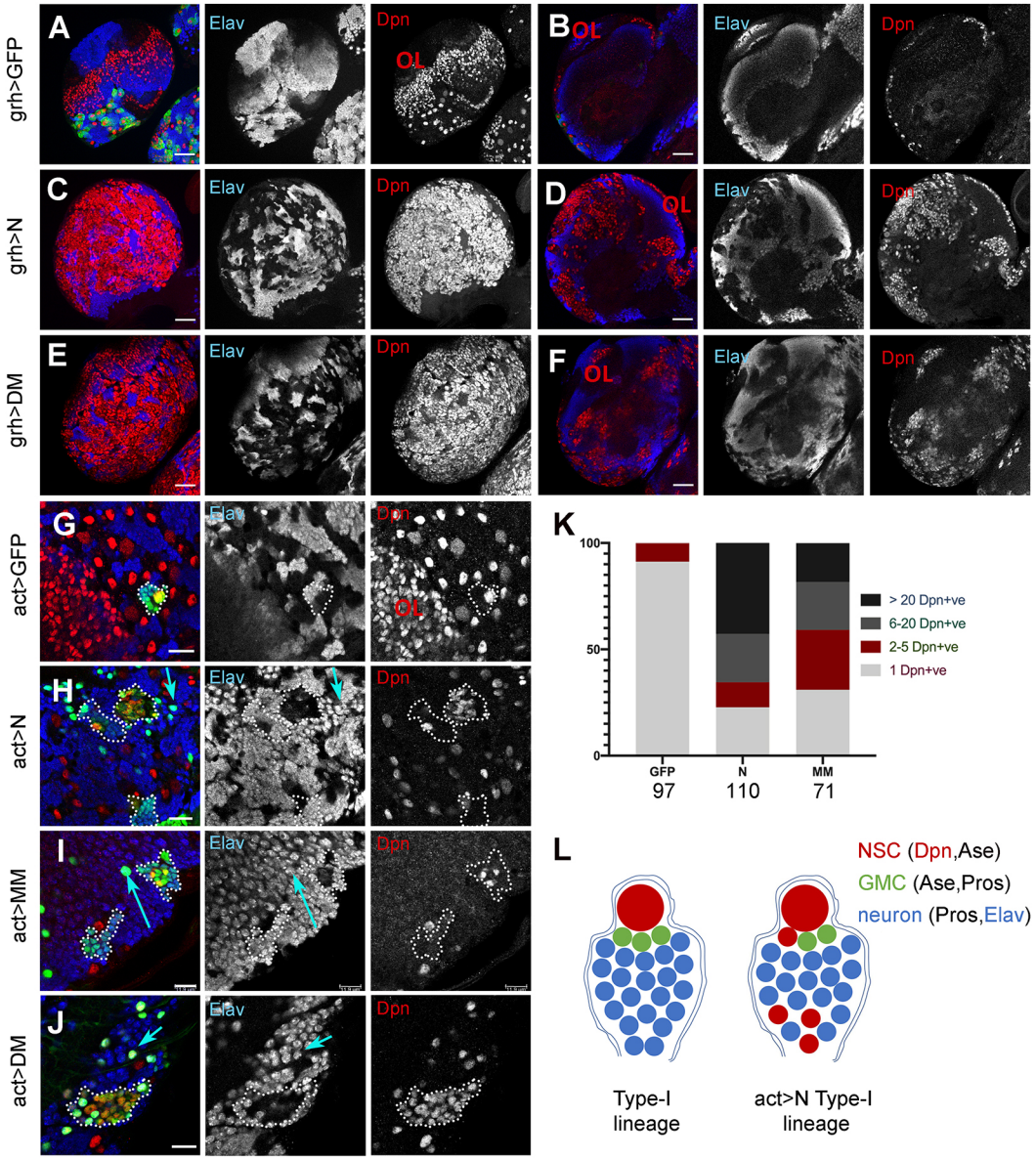

Fig. 1. Hes proteins induce neural hyperplasia. (A-J) Staining for NSCs (Dpn, red) and neurons (Elav, blue). (A,B) *grhNB-Gal4; UAS-CD8GFP* brain lobe; (C,D) Brain lobe from *atub-Gal80ts; grhNB-Gal4; UAS-NΔecd* exposed to the restrictive temperature for 24 h; (E,F) Brain lobe from *grhNB-Gal4; UAS-dpn, UAS-mγ*. A,C,E show superficial projections of ∼8 µm; B,D,F are deep single sections at the level of the neuropil. (G-J) Superficial confocal sections of Type-I lineage *act>stop>Gal4* FLP-out clones expressing the indicated transgenes; G,H are from brain lobes and I,J are from VNCs. NSC lineage clones are traced by dotted lines. Examples of single-cell clones are marked by blue arrows. (K) Number of Dpn-positive cells per clone in the genotypes shown in G-I. Numbers of Type I lineage clones scored at 3 days after clone induction are indicated. (L) Schematics of wt versus *NΔecd*-overexpressing Type I lineages. *DM* lineages are similar, with the exception of ubiquitous Dpn expression. *MM* lineages are also similar, with the exception of frequent detection of cells that express neither Dpn nor neuronal markers. OL, optic lobe. Scale bars: 50 µm in A-F; 25 µm in G-J.

after transplantation showed broad expression of nuclear Dpn. In addition, several cells were positive for nuclear Pros (GMC/early neuron-like; Fig. 2C,D), while Elav-positive neuron-like cells were also observed more sparsely (examples shown later in Fig. 10). These more differentiated cells had generally low or undetectable levels of Dpn, although double-positive cells were also occasionally seen (Fig. 2C). These results indicate an NSC-like tumour phenotype with sustained proliferation (Fig. 2E) and little differentiation.

Comparison of transcriptomes from different CNS primary tumours

As both Hes overexpression and Notch overactivation produce NSC tumours, we wanted to find out to what extent the CNS transcriptomes following these insults are similar or different. For this reason we performed microarray analysis using RNA from hand-dissected CNSs exposed for 24h (by heat-inactivating the *αtub-Gal80ts* inhibitor of Gal4) to *DM*, *MM* or *dpn* (*D*) overexpression via *grhNB-Gal4*. We compared these to Notch- and GFP- (control) overexpressing CNSs using the same overexpression regimen (Zacharioudaki et al., 2016). For this analysis we decided to focus on the *N* and 2xHes combinations (*DM* and *MM*), as these gave the strongest hyperplasias. Out of 8479 probesets with detectable expression in control larval CNS, we found 1410 that were differentially expressed by at least 1.8× at a FDR≤0.05 in at least one of these three conditions (Fig. 3A; Fig. S7). *MM* and *DM* showed very similar transcriptomes – of the 1410 differentially expressed genes (DEGs), none showed an opposite trend between these

Development (2020) 147, dev191544. doi:10.1242/dev.191544

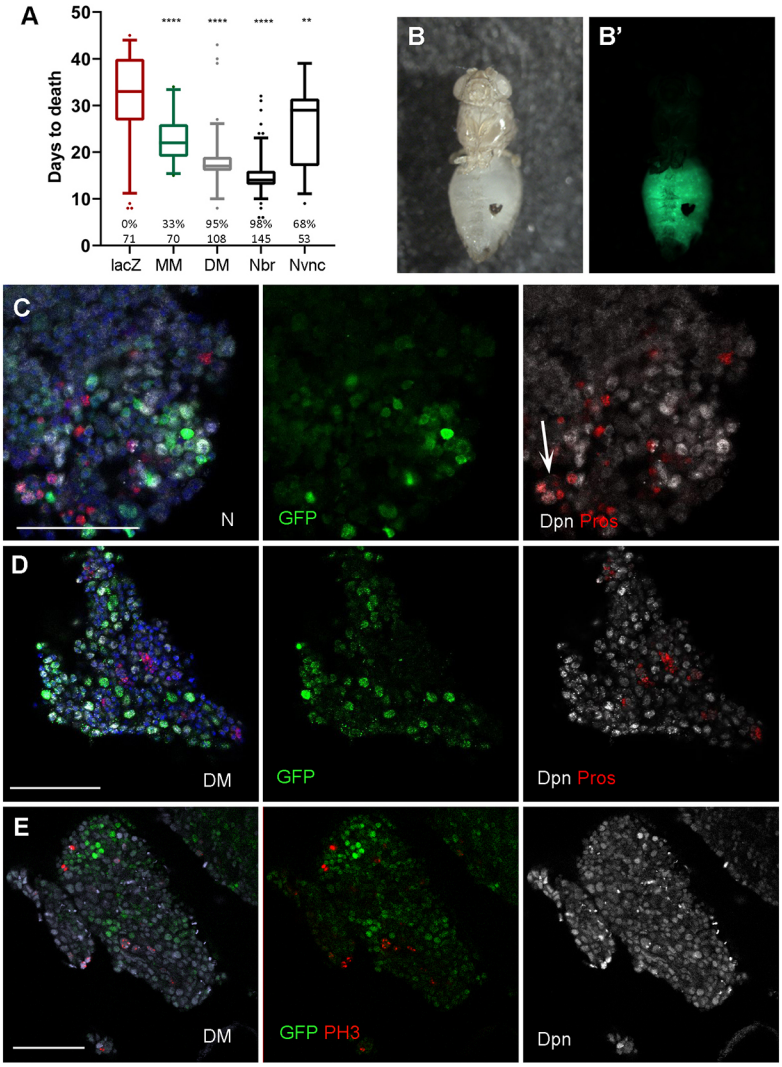

Fig. 2. *NΔecd* and Hes overexpression generates transplantable tumours. (A-E) Single VNCs (Nvnc, N-expressing) or brain lobes (all others) containing *act>stop>Gal4* induced clones overexpressing *lacZ* (control), *N*, *DM* or *MM* were allografted into adult wt female abdomens. Quantification in A shows host lifespan after transplantation [box-plot: median values (middle bars) and first to third interquartile ranges (boxes); whiskers are 5% and 95%; dots indicate outliers]. ***P*<0.01; *****P*<0.0001 (unpaired *t*-test). The numbers indicate the sample size scored. Only flies that developed GFP (as in B) were scored, except for the *lacZ* control. Percentages show the fraction of allografted flies that developed GFP. B shows brightfield image and B′ shows epifluorescence image of one indicative host injected with an *act>N* brain. C-E shows fragments of tumour recovered from allografted host abdomens and stained for the markers shown. Histone H3-phosphoS10 (PH3, red) is a mitotic marker, DAPI (blue) shows nuclei. The arrow in C points to a group of double Dpn/Pros-positive cells. Scale bars: 50 µm.

two conditions (up in one and down in the other). The *N* transcriptome was more distinct, but even so, only a very small number of probesets (eight) showed an opposite trend between *N* and *MM/DM* (union of DEGs in *MM* and *DM*). Correlation analysis showed that Hes tumours, including the weaker *D* (*dpn* alone), are more similar to each other than to the Notch tumour (Fig. 3D). In conclusion, Hes gene overexpression causes dramatic transcriptome changes in the CNS, which bears similarities and differences to that caused by *NΔecd* overexpression.

To address whether our transcriptome changes simply reflect the change in cellular composition of the CNSs used, we asked whether they correspond to upregulation of NSC-specific genes and/or downregulation of neuron-specific genes. When we queried a list of genes differentially expressed in wt NSCs versus neurons (Berger et al., 2012), no such trend was observed. Instead, most neuron- and NSC-enriched genes were unchanged in the *N*/Hes CNSs and conversely most *N*/Hes differentially regulated genes belonged to neither the neuron- nor the NSC-enriched genesets (Fig. S8). Similar results were obtained with a more recent categorization of genes expressed differentially between (wt) NSCs and GMCs (Wissel et al., 2018). We conclude that the transcriptomic changes that we documented are mostly due to the deregulation of the Notch/Hes axis and less because of the accompanying over-representation of NSCs versus GMCs and neurons.

Other genetic insults have been reported to generate brain tumours in *Drosophila* (reviewed by Kang and Reichert, 2015). We recovered transcriptome data for two tumours formed by *brat* RNAi in NSC lineages (using *insc-Gal4*) (Neumüller et al., 2011), two caused by the loss of cell polarity genes *l(2)gl* and *scrib* (GEO GSE48852) and one caused by the loss of the nuclear architecture gene *l(3)mbt* (Janic et al., 2010). When we compared these with our *N*/Hes-induced tumours (Fig. 3D; Fig. S9), we saw little or no similarity. Essentially no correlation was observed between the Hes transcriptomes and any of the other tumours. The *N* transcriptome showed a moderate correlation with the two *brat* RNAi conditions, but not the $l(2)gl^{-/-}$, $scrib^{-/-}$ or $l(3)mbt^{-/-}$. This is consistent with the fact that the *N*/Hes tumours consist mostly of NSC-like cells, whereas the $l(2)gl^{-/-}$ and $scrib^{-/-}$ tumours strongly express differentiation markers (Beaucher et al., 2007). *l(3)mbt* tumours stood apart from all others, in agreement with a different cellular origin (optic lobe precursors; Richter et al., 2011). In short, Notch overactivation partially resembles Hes overactivation and partially resembles *brat* loss-of-function, which are distinct from each other.

Upon GO term analysis of the *N*/Hes transcriptomes, a few terms showed statistically significant enrichment (Fig. 3B,C), mostly associated with neurogenesis. Interestingly, ‘DNA binding transcription factor’, was enriched in both the upregulated and

Development (2020) 147, dev191544. doi:10.1242/dev.191544

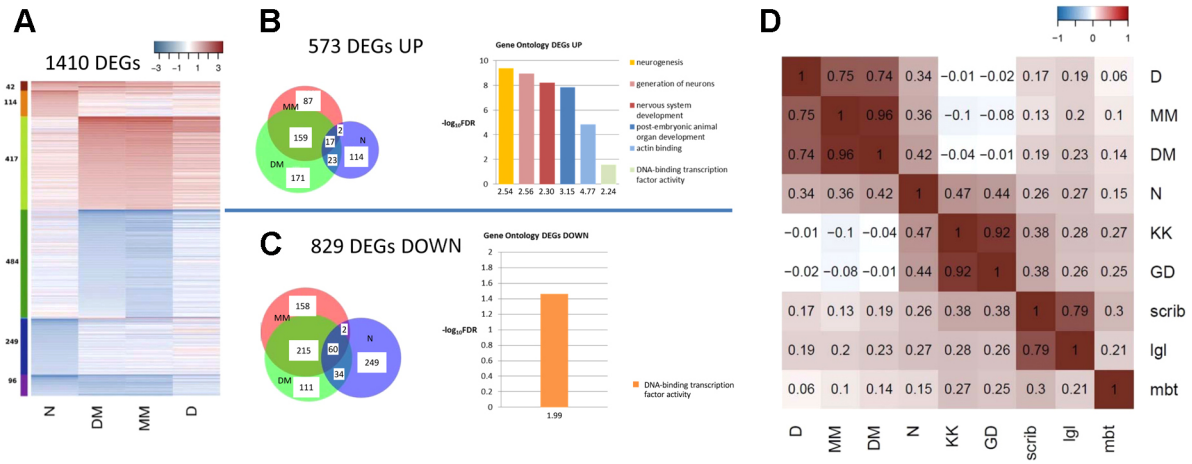

Fig. 3. Microarray analysis of Notch versus Hes overexpressing larval CNSs. (A) Heatmap showing the $\log_2$(fold-change) of all 1410 genes (probesets) with an expression change of at least 1.8× compared with wt CNS controls (FDR≤0.05) in at least one of the four conditions (*N*, *DM*, *MM* or *D* expressed by grhNB-Gal4 for 24 h). (B,C) The 1410 DEGs were split into 573 upregulated (B) and 829 downregulated (C) (and eight oppositely regulated; GSE141794). The Venn diagrams classify these genes according to the condition(s) where they showed change with high confidence (FDR≤0.05). GO terms showing significant enrichment are shown with fold enrichment in the *x*-axis. (D) Spearman rank correlation coefficients of the distributions of fold-change values for nine CNS tumour transcriptomes, calculated on the basis of the entire set of 8479 genes, showing detectable expression in our control array. scrib, lgl and mbt refer to homozygous mutant CNSs for *scrib*, *l(2)gl* and *l(3)mbt*; KK and GD refer to two *brat* RNAi lines driven by *insc-Gal4*.

downregulated subset of DEGs, which prompted us to focus on TF genes for the follow up analysis.

Genome-wide binding of Dpn

Transcriptomic analysis of complex tissues is inherently noisy from the contribution of numerous cell types. In order to reveal the direct targets of Hes proteins in the NSCs we performed ChIP using an anti-Dpn antibody on hyperplastic larval CNSs overexpressing *UAS-dpn+UAS-E(spl)mγ* driven by *grhNB-Gal4*. This enabled us to focus on the expanded population of NSCs, as there is little Dpn expression (endogenous or transgenic) in other cell types. From two ChIP-seq biological replicates we obtained a high confidence set of 229 regions displaying Dpn occupancy (Fig. 4A). Mining these 229 ChIP peaks for over-represented DNA motifs, we obtained an E_B/E_C box sequence and variants as the top hits (Fig. 4B), confirming that in an *in vivo* context Dpn binds sequences that conform to the well described *in vitro* binding consensus for Hes proteins (Jennings et al., 1999; Winston et al., 1999).

A large percentage of the Dpn peaks fell within or near genes (Fig. 4C). We extracted a list of 358 genes that contain at least one Dpn binding event within ±5kb of the gene body. These genes are enriched for factors involved in neural precursor development, Notch signalling and transcriptional regulation (Fig. 4D). When this list of Dpn binding-associated genes was overlapped with the DEGs from the microarray experiment, we obtained 50 genes, the transcriptional response of which is shown in Fig. 4E. Although Hes proteins are thought to act as repressors, only half of these 50 Dpn-bound genes showed repression in the Hes-induced tumours. This is not surprising, because of the heterogeneity of the tissue analysed and the complexities of transcriptional regulation. Genes bound by Dpn in the NSCs may also be expressed in cell types other than NSCs/GMCs/early neurons, in which we drive DM overexpression. Furthermore, mRNA levels respond to multiple transcriptional/post-transcriptional regulatory inputs, so that the overall effect of Hes overexpression (integrating direct and indirect effects) may not be repression, despite Dpn binding near these genes. We do not exclude the possibility that Hes proteins might behave as activators in certain enhancer contexts, although we have no evidence in support of such a scenario (Fig. S10). We focussed our subsequent experimental validation on a set of TF genes which appear to be prominent Hes targets, as they combine high Dpn occupancy with transcriptional repression in the Hes-induced tumours.

Differentiation-promoting TFs are among the most highly downregulated Hes target genes

Amongst the top downregulated/Dpn-bound transcription factors we noted two zinc-finger genes *erm* and *nerfin-1*, known to promote neural differentiation (Fig. 4E,H,I). *erm* is turned on in the immature INP progeny of Type II NSCs and restricts their self-renewal. Its loss-of-function is sufficient to cause dedifferentiation of INPs to highly proliferative ectopic Type II NSCs (Janssens et al., 2014; Koe et al., 2014; Weng et al., 2010). An enhancer recapitulating its expression was shown to bind stem cell repressors, including Dpn (Janssens et al., 2017) and coincides with one of the two peaks we detected (Fig. 4H). *nerfin-1* is expressed in newly born neurons in both Type I and II lineages as well as in terminating NSCs after pupariation. Its loss can cause dedifferentiation and overproliferation (Froldi et al., 2015).

Besides, the well-studied *erm* and *nerfin-1*, there were another 13 TFs among the 27 downregulated/Dpn-bound TF genes. We chose two of these, *zfh1* and *gcm* (Fig. 4F,G), as they had been implicated in differentiation (see below) and we had access to reagents, to ask whether their repression by the *N*/Hes system might play a role in NSC tumorigenesis. *zfh1* encodes a large protein with a homeodomain and nine zinc-fingers; it has a broad tissue distribution and pleiotropic functions, e.g. embryonic mesoderm, neuron and glia differentiation (Layden et al., 2006; Postigo et al., 1999; Sellin et al., 2009). In third instar larval and early pupal CNSs we detected moderate expression in newly-born neurons in most brain (Type I and II) and VNC lineages (Fig. 5A,B, yellow arrows). Stronger expression was detected in dispersed older neurons located in deeper cortical layers (Fig. S11). In addition, a large number of glia, perhaps all glia, exhibited detectable *zfh1* expression. Hyperplastic brains generated by overexpression of *NΔecd* or *2xHes* using *grhNB-Gal4* showed reduced *zfh1* expression, especially in the superficial layers (Fig. 5C-F). The disorganization of the brain and shrinking of the neuropils did not allow us to assess the effect on mature neurons and glial cells.

Development (2020) 147, dev191544. doi:10.1242/dev.191544

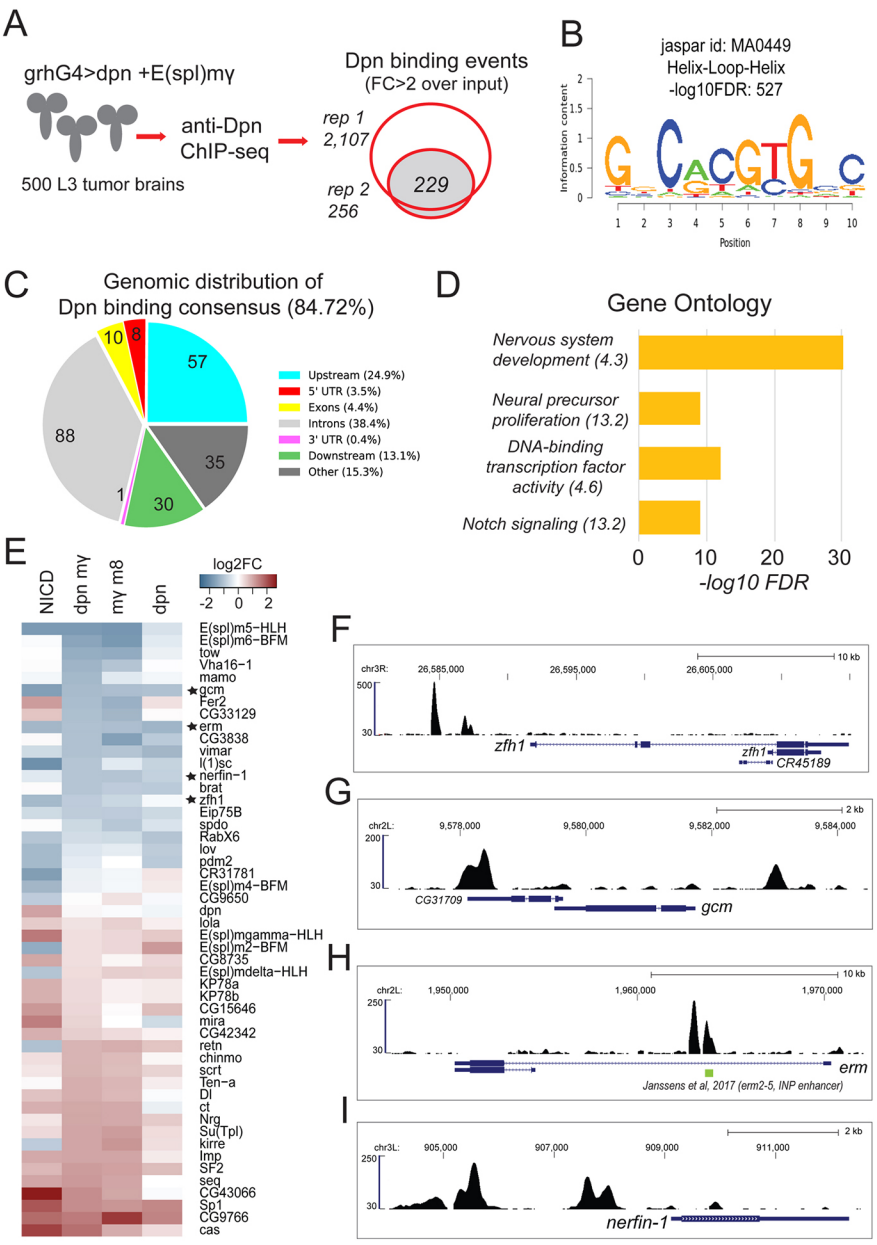

Fig. 4. Genome-wide mapping of Dpn binding in *DM* CNS hyperplasias. (A) Chromatin extracts from 500 third instar larval *DM* CNSs were isolated and incubated with anti-Dpn bound beads. A Dpn binding consensus of 229 binding events was generated from regions enriched at least 2× input in two biological ChIP replicates. (B) Motif analysis of the Dpn-bound regions revealed high enrichment for a Hes-type bHLH binding motif. (C) Genomic distribution of Dpn-bound peaks. (D) Gene ontology enrichment analysis of the 358 genes with Dpn binding events in their vicinity. (E) Transcriptional response of 50 Dpn-bound genes that were also differentially regulated in our microarray analysis. (F-I) Genomic snapshots of Dpn binding at the *zfh1* (F), *gcm* (G), *erm* (H) and *nerfin-1* (I) loci.

The *gcm* gene encodes a transcriptional activator and founder of the Gcm-family of proteins, which are known to promote gliogenesis (Ragone et al., 2003), but also differentiation of some neurons, tendon cells and haemocytes (Cattenoz et al., 2016). In the larval CNS we detected *gcm* expression using the gcm^{rA87}-*lacZ* enhancer trap (Jones et al., 1995) (Fig. 6). Besides widespread expression in the optic lobe, there was sparse expression in the larval CNS (Fig. 6A,B). In deep areas (near the neuropils) *lacZ* was detected in some Repo-positive glial cells as well as nearby cells that could be neuropil glia precursors (Fig. S12). At the superficial levels of the central brain and thoracic ganglion, we did not detect *lacZ* expression in NSCs, but we did detect it in some INPs in both lateral and medial Type II NSC lineages (Fig. S12). This is in agreement with the fact that some of the Type II lineages produce glia as well as neurons (Viktorin et al., 2011, 2013). *gcm-lacZ* was also prominently expressed in two neuronal clusters, one on the ventral and one on the dorsal side of each brain hemisphere – these are Type I-derived neurons, but nearby NSCs were *gcm-lacZ*-negative (Soustelle and Giangrande, 2007). The only NSCs expressing *gcm-lacZ* were found at the medial edge of the medulla and at the optic lobe inner proliferation centre (Fig. S12A,C), probably gliogenic NSCs (Li et al., 2013). Upon *grhNB-Gal4* overexpression of *2xHes* or *NΔecd*, central brain expression of *gcm-lacZ* was downregulated in both neuron and glial precursors (Fig. 6C-F), with the exception of some deep glial precursors that retained *gcm-lacZ* expression. Optic lobe expression was unaffected, as *grhNB-Gal4* does not drive expression in the optic lobe.

Loss- and gain-of-function analysis of novel Hes targets

Both embryonic and post-embryonic phenotypes of the loss of *gcm* and *zfh1* have been described. *gcm* loss-of-function in the larva results in the absence of most glial cells born post-embryonically (Awasaki et al., 2008). In the postembryonic CNS, *zfh1* loss-of-function has been studied in the context of specific leg motor neuron lineages and it results in defects in neuron morphology, but not defects in their birth or neurotransmitter phenotype (Enriquez et al., 2015). To address their need in NSCs and their immediate progeny,

Development (2020) 147, dev191544. doi:10.1242/dev.191544

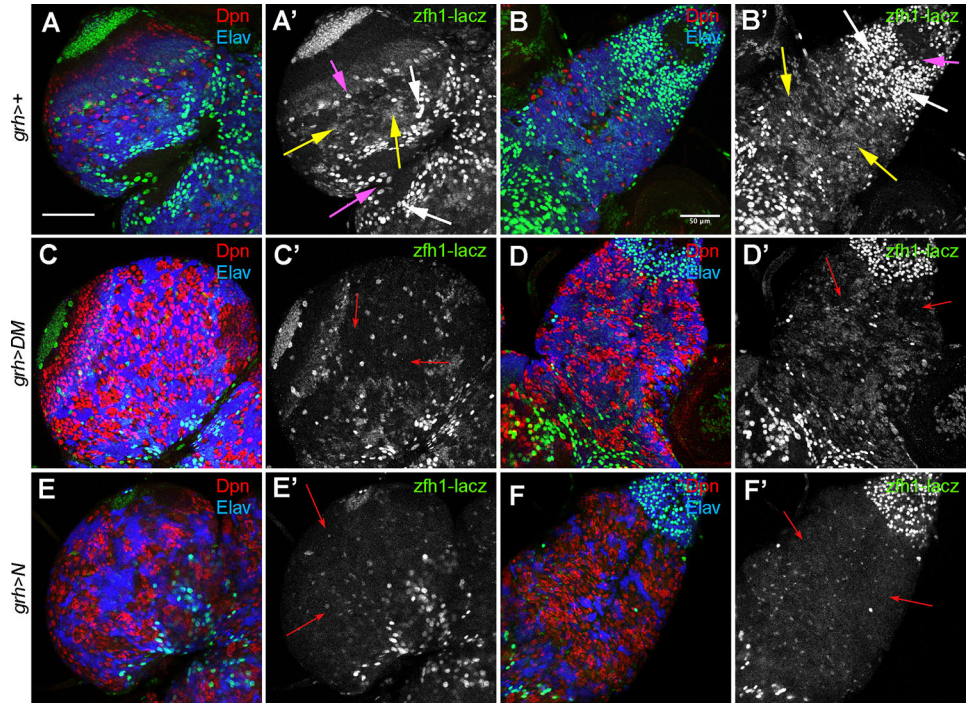

Fig. 5. *zfh1* expression in wt and hyperplastic CNSs. (A-F) *zfh1-lacZ*^{00865} was used to report *zfh1* expression (green), compared with Dpn (red) and Elav (blue). Panels show ∼2 µm-thick projections just below the CNS surface from brain lobes (A,C, E) and VNCs (B,D,F). All CNSs carry *grhNB-Gal4* and no UAS transgene (wt) (A,B), *UAS-dpn, UAS-E(spl)mγ* (*DM*) (C,D) and *UAS-NΔecd* (*N*) (E,F). In the wt panels (A-B′), regions of *zfh1*-expressing GMCs/young neurons are marked with yellow arrows, selected mature neurons with white arrows and selected glia with magenta arrows. In C′-F′, examples of regions of *zfh1* repression are indicated by red arrows. Scale bars: 50 µm.

we generated MARCM clones for null alleles (*zfh1*$^{75.26}$ or *gcm*$^{N7-4}$) 24-48 h after larval hatching and studied their effects 3-5 days later, namely in late larval or early pupal (12-24 h after puparium formation) stages. Unlike *erm* and *nerfin-1*, the loss of which causes supernumerary Type II and Type I NSCs, respectively, knocking out either *zfh1* or *gcm* had no detectable effect in the cellular composition of either Type I or Type II lineages based on NSC, GMC and neuron markers (Dpn, Pros, Elav; Fig. S13).

We then turned to a gain-of-function approach to ask what would happen if we were to forcibly express these Hes-repressed factors in NSCs. For this reason we used an *act>STOP>Gal4* driver and induced expression by *hs-FLP* in mid-larval stages. Overexpression of *zfh1* in type I lineages resulted in complete elimination of Dpn within 1 day of clone induction (Fig. 7A-D,G). This was accompanied by shrinkage of the NSC, making it in most cases (76% of the clones) indistinguishable from other cells in the clone. Ase, another NSC (and GMC) marker, was not similarly repressed within the first day, although it too was extinguished at later times after clone induction (ACI) (Fig. S14). Interestingly, Elav and Pros were also partially repressed in *zfh1*-overexpressing lineages (Fig. 7C-F; Fig. S14): several cells lacked both Dpn and these differentiation markers in a large proportion of clones (Fig. 7H). For

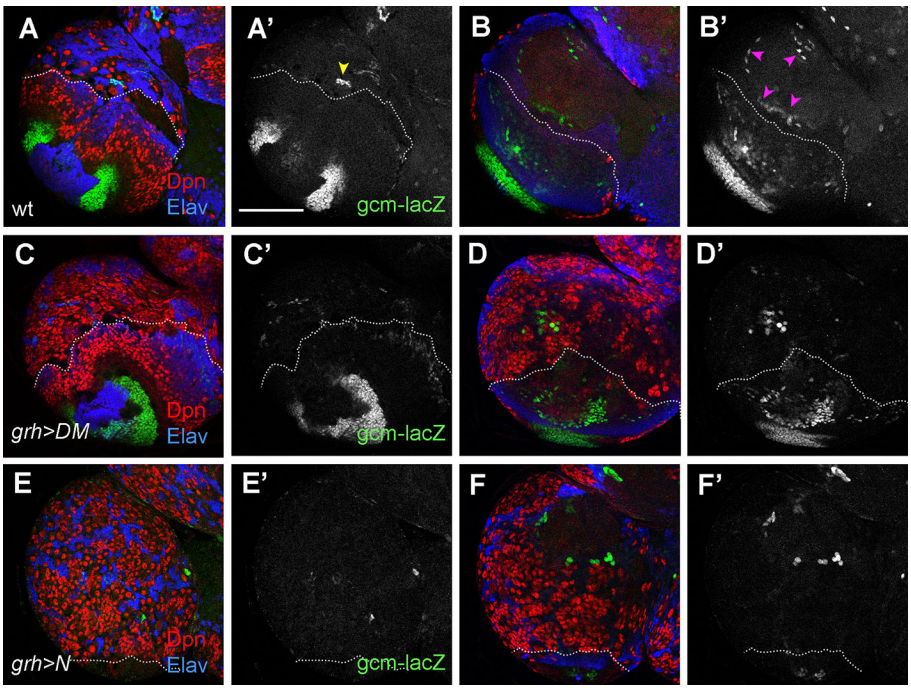

Fig. 6. *gcm* expression in wt and hyperplastic CNSs. (A-F) *gcm-lacZ*^{rA87} was used to report *gcm* expression (green) versus Dpn (red) and Elav (blue). (A,B) wt brain lobe, superficial (A) and deep (B) section. Neuropil glia are indicated by magenta arrowheads. One of the Gcm-positive neuronal clusters is marked by a yellow arrowhead. (C,D) *DM*-overexpressing brain lobe, superficial (C) and deep (D) section. (E,F) *N*-overexpressing brain lobe, superficial (E) and deep (F) section. In all panels, the dotted line indicates the border between central brain (upper) and optic lobe (lower). Scale bar: 100 µm.

Development (2020) 147, dev191544. doi:10.1242/dev.191544

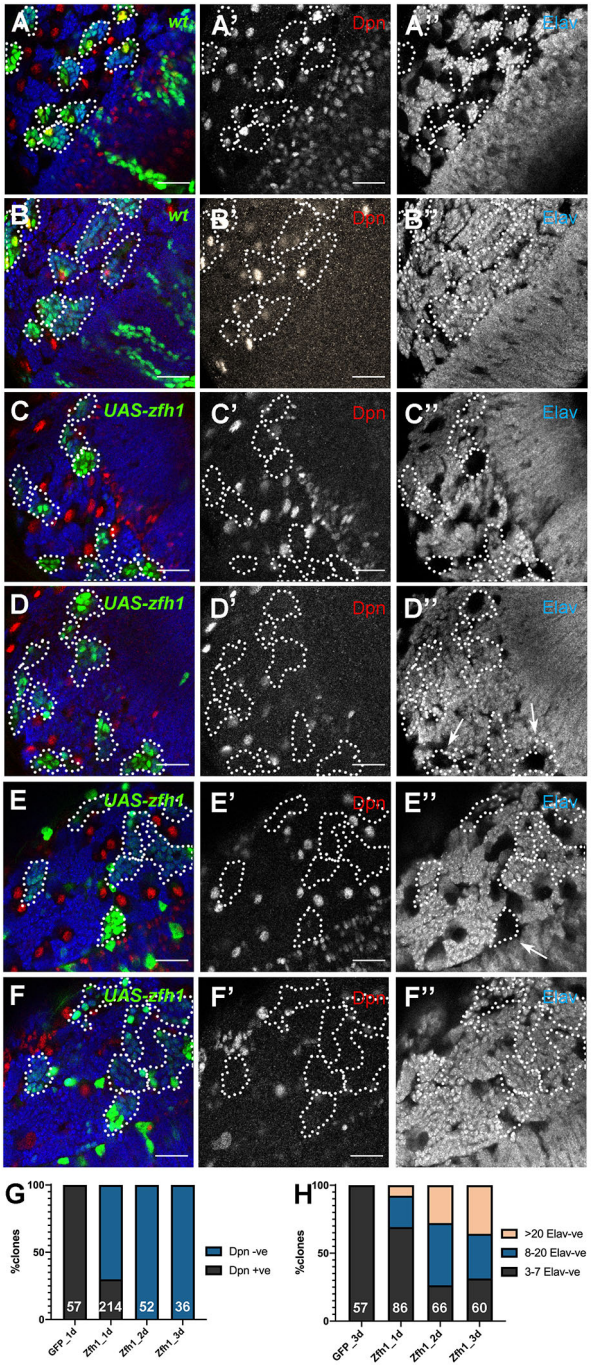

Fig. 7. *zfh1* misexpression in CNS lineages. (A-F) *act>STOP>Gal4* FLP-out clones are marked by GFP (green) and traced with dotted outlines. (A,B) Control (wt) clones, 2 days after clone induction (ACI) – the same brain lobe area imaged superficially, at the level of NSCs (A) and deeper (B). (C,D) Superficial and deep sections (same region) of *UAS-zfh1* clones 1 day ACI. (E,F) Superficial and deep sections (same region) of *UAS-zfh1* clones 2 days ACI. Arrows (D″,E″) point to examples of Elav-repressed clones. Scale bars: 25 µm. (G) Frequency of clones containing or lacking a Dpn-positive cell. (H) Frequency of clones showing extensive Elav repression or exhibiting normal Elav in all cells but the NSC/GMCs.

comparison, wt clones never contained Dpn/Pros-double negative cells; nuclear Pros was detectable in all NSC progeny (GMCs and neurons) and Elav gradually came on in neurons, even those that were still close to the NSC at the CNS surface. Thus overexpression of *zfh1* was able to antagonize both NSC and neuron cell fates. These cells were not converted to glia, as the glial marker Repo was not induced in *act>zfh1* clones (Fig. S14).

Unlike *zfh1*, ectopic expression of *gcm* for 2-3 days did not greatly upset the execution of NSC lineages, other than converting some of the differentiated progeny into glia (Fig. S15; see also Fig. 9E), consistent with its well-known glia-promoting role.

Overexpression of Hes targets ameliorates the tumour phenotype

We next wanted to address whether overexpression of *zfh1* or *gcm* would influence *N*/Hes-induced tumorigenesis. If the depletion of these Hes targets contributes towards tumorigenesis in Hes/Notch CNS tumours, perhaps expressing them transgenically would reverse this effect. We therefore co-expressed either *gcm* or *zfh1* with tumour-promoting transgene combinations, namely *N*, *MM* or *DM*, in random *act>STOP>Gal4* clones.

Overexpression of *zfh1* in a tumour background produced round clones with a conspicuous absence of Dpn in most lineages (unless *UAS-dpn* was used); only a few scattered escaper Dpn-positive cells were seen (Fig. 8). Therefore, the ability of Zfh1 to repress *dpn* overrides the activation of the latter by *N* or *MM*. Another NSC marker, Ase, responded more variably: it was fully repressed in *UAS-N+zfh1* clones, whereas it showed variable penetrance in *UAS-DM* (or *MM*)*+zfh1* clones (Fig. S16): in some clones it was repressed, whereas in others it was activated in many cells. More remarkable was the strong repression of Elav (Fig. 8) and Pros (Fig. S16) in *UAS-N* (*DM*, *MM*)*+zfh1* clones, which was seen with full penetrance (in all clones) in the majority of the marked cells. Whereas both *UAS-N* (or *DM* or *MM*; Fig. 1) and *UAS-zfh1* (Fig. 7) produced sporadic loss of these differentiation markers, their combination was far more potent (compare Fig. 8A,C,E with Fig. 8B,D,F). We excluded the possibility that the *N*/Hes*+zfh1* expressing cells were massively converted to glia using the pan-glial Repo marker (Fig. S16). In summary, *zfh1* overexpression overrides Dpn induction by *N*/Hes (Fig. 8G), but synergizes with the latter to maintain CNS progenitors in an undifferentiated state (which sometimes retain the Ase marker), generating cell clumps that stay separate and do not integrate with the cortex of differentiated neurons/glia.

Overexpression of *gcm* had a markedly different effect in *N* versus *DM* tumour backgrounds (Fig. 9; Fig. S17). In the *N* background it enhanced neuronal de-differentiation, with fully penetrant repression of Elav, but little or no repression of Pros (Fig. S17A,C). Repo was dramatically induced and often co-expressed with Dpn (Fig. 9A,B). More specifically, *N+gcm* clones consisted mostly of two types of cells: NSC-like Dpn-positive/Repo-negative cells and Dpn/Repo-double positive cells with lower Dpn levels. In contrast, *gcm+Hes* co-expression did not induce Repo as strongly; only a few cells were Repo positive in 10-20% of the clones, which is less than the frequency of Repo induction by misexpression of *gcm* alone (Fig. 9C-E). *DM*/*MM+gcm* also did not enhance Elav repression beyond that caused by *DM* or *MM* alone (Fig. S17B). Instead, it reduced the NSC-like cells, as evidenced by a reduction in Ase- or Dpn-positive cells compared with *DM*/*MM* alone (Fig. S17D-H). In conclusion, whereas *gcm* synergizes with Notch to generate precursor-like cells, many of which express the glia marker Repo, this cannot be recapitulated by co-expressing *gcm* with Hes factors, suggesting a different mechanism of Notch-Gcm synergy that may not involve the usual Hes targets of Notch.

To determine the malignancy potential of NSC tumours after co-expression of *zfh1* or *gcm*, we transplanted brain lobes bearing *N* or *DM* clones into abdomens of adult females. Both *zfh1* and *gcm*

Development (2020) 147, dev191544. doi:10.1242/dev.191544

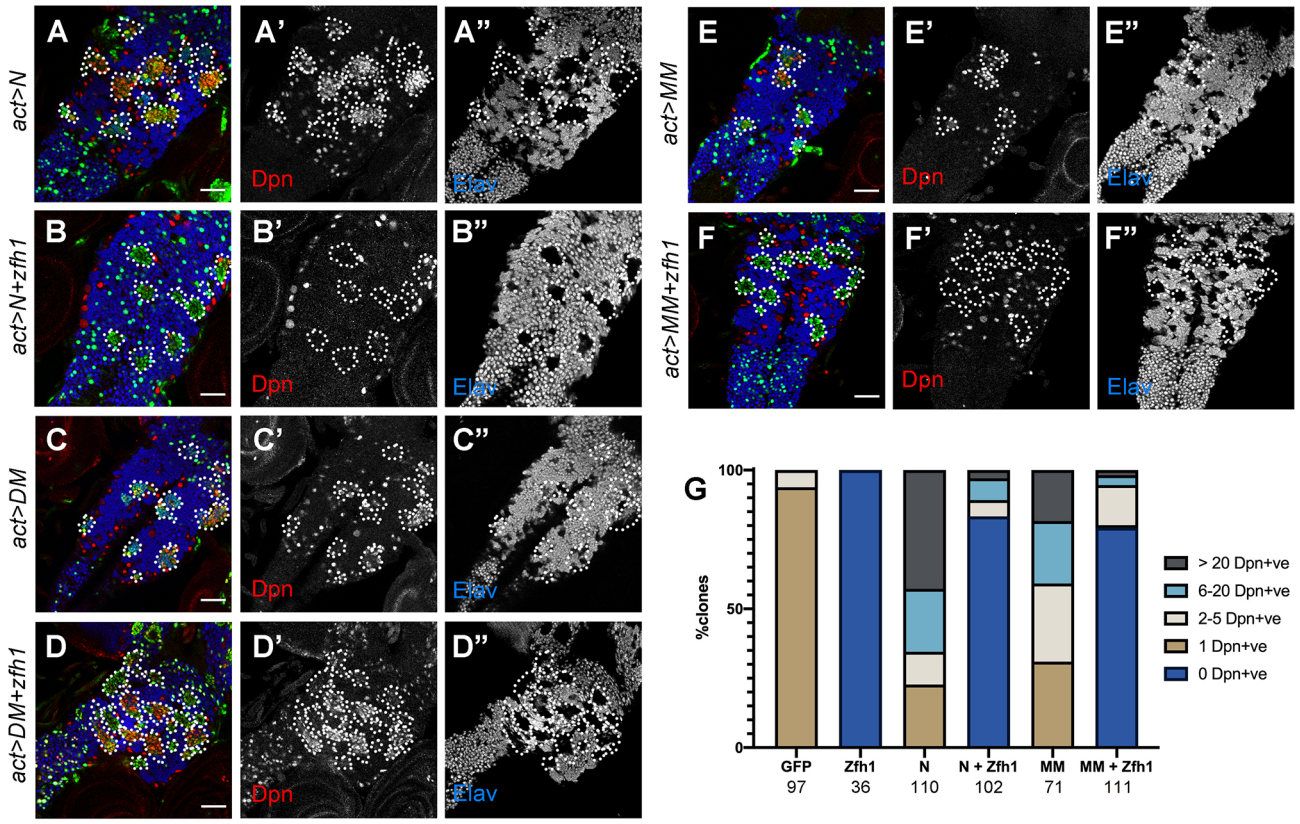

Fig. 8. Effects of *zfh1* misexpression on *N*, *DM* and *MM* lineages. (A-F) FLP-out (*act>STOP>Gal4*) clones (traced by dotted lines) expressing GFP (green) and the indicated transgenes. (A′-F′) Dpn channel and (A″-F″) Elav channel. All images are from VNCs; the same effects were observed in brain lobes. Scale bars: 50 µm. (G) 3-day-old (ACI) clones were scored for the number of NSCs per clone. The total number of Type I clones (both brain lobes and VNCs) scored for each genotype is shown below the chart.

significantly decreased the number of allografts generating malignancies from ∼100% to 77% or less (Fig. 10A). Many of these tumours grew more slowly and allowed their hosts to survive longer (Fig. 10A). Therefore, both *zfh1* and *gcm* have an anti-tumorigenic effect when co-expressed with *N* or *DM*. Upon histological examination of *N+zfh1* tumours, we observed a large number of Elav-positive (neuron-like) cells, which were only sporadically seen in *N* tumours. Intriguingly, when the malignant tumour from the original allograft (T0) was transplanted to a new host, the resulting tumour (T1) contained significantly fewer Elav-positive cells and this was also true for T2, the next passage (Fig. 10B-G). Therefore, the *N+zfh1* CNS lineages have a greater tendency to differentiate after allografting (despite their initial repression of Elav), but they lose this ability upon serial passaging.

DISCUSSION

During neurogenesis, NSCs divide asymmetrically and their more differentiated progeny sends a Dl-Notch signal back to the NSC. We have studied the NSC hyperplasias caused by overactivation of Notch or overexpression of its Hes targets, *dpn*, *E(spl)mγ* and *E(spl)m8*, in the larval CNS of *Drosophila*. Here, we show that such ectopic NSCs are highly prone to malignancy, as evidenced by their ability to be serially allografted and propagated in adult hosts. The proliferating larval NSCs and their progeny were already known to be prone to tumorigenesis if their asymmetric cell divisions are perturbed (Caussinus and Gonzalez, 2005; Gateff, 1978). Tumorigenesis has been more recently documented for other insults, among others overexpression of the early temporal TF *chinmo* (Narbonne-Reveau et al., 2016) or loss of the differentiation TF *nerfin-1* (Froldi et al., 2015). It was suspected that Notch overactivity would also be tumorigenic based on the malignancy of *numb* loss-of-function lineages (Caussinus and Gonzalez, 2005), and we now firmly show that indeed Notch/Hes axis overactivity can lead to CNS tumorigenesis.

How does the Notch/Hes axis contribute to NSC maintenance? Earlier we showed that Su(H), the TF that tethers cleaved (activated) Notch to its target enhancers, binds near all genes specifically expressed in the larval NSC, indicatively *klu*, *ase*, *wor*, *pnt*, *Myc* and *mira*, besides the Hes genes in the *dpn* and E(spl) loci (Zacharioudaki et al., 2016). This is consistent with Notch signalling promoting NSC maintenance and with the fact that one of the steps taken by the differentiating NSC progeny is to downregulate the Notch signal by accumulating high levels of Numb, a Notch inhibitor. In fact the phenotype of our *act≫Gal4* (FLP-out) clones overexpressing *NΔecd* or *2xHes* (Fig. 1) is almost identical to the phenotype of $numb^{-/-}$ clones (Lin et al., 2010).

From our earlier analysis, we knew that Hes genes are needed for NSC maintenance (Zacharioudaki et al., 2012). In the present work, we have gained insight on how the Hes factors contribute to NSC maintenance. We have shown that Dpn binds and represses a number of TF genes, among which are some that promote differentiation. A typical one is *gcm*, a well-known glia-promoting TF, which was able to antagonize Notch/Hes-induced tumorigenesis (Fig. 10). Another Hes-repressed direct target is *zfh1*, which appears to reciprocally repress *dpn* (Fig. 7), although we do not know whether this is a direct or indirect effect. Previously, genetic interactions implicated Zfh1 in the action of the NURD chromatin remodelling complex, which was shown to

Development (2020) 147, dev191544. doi:10.1242/dev.191544

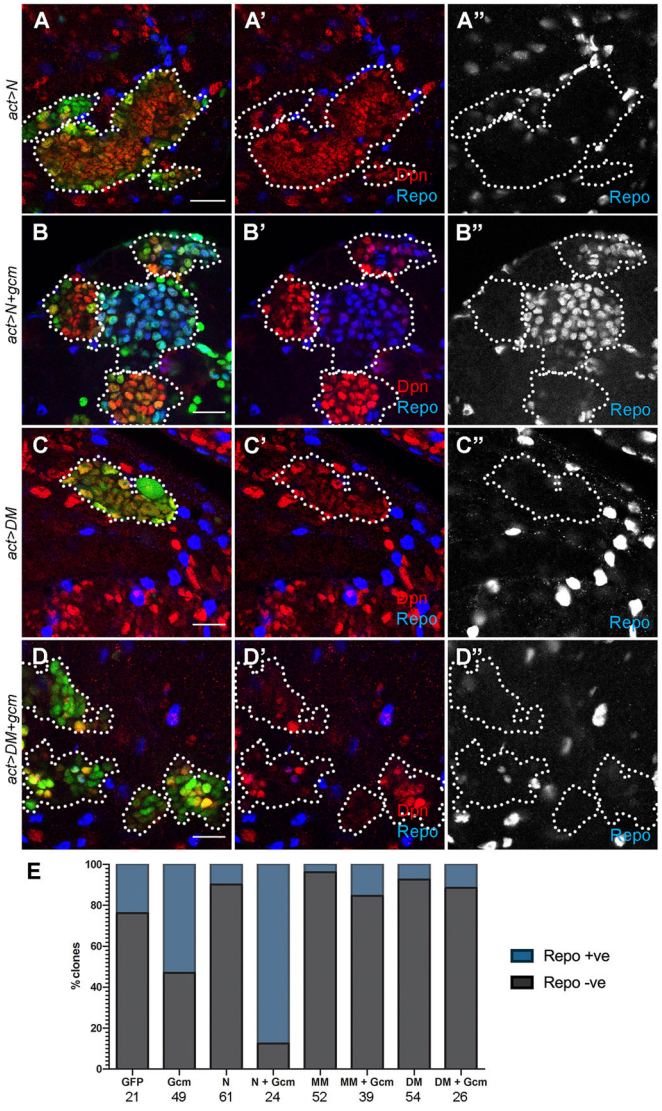

Fig. 9. Effects of *gcm* misexpression on *N* and *DM* lineages. (A-D) FLP-out (*act>STOP>Gal4*) clones (traced by dotted lines) from brain lobes expressing GFP (green) and the indicated transgenes. Repo (blue) marks glial cells. Note the general scarcity of Repo-positive cells within clones, with the exception of (B), in which two clones contain large numbers of glia. Scale bars: 20 µm. (E) The frequency of clones containing at least one Repo-positive cell (blue) versus none (grey). The numbers below the chart indicate the number of clones scored. Only clones in central brain regions were scored.

shut off *E(spl)mγ* transcription in NSC progeny (Zacharioudaki et al., 2019). A plausible scenario is that Zfh1 acts with NURD to actively decommission many Notch-responsive target enhancers in NSC lineages, including *dpn* and E(spl). Besides repressing Hes genes, Zfh1 must also have other NSC targets, as its forced expression ameliorates *DM* tumorigenesis, despite exogenous expression of *dpn* and *E(spl)mγ* (Fig. 8; Fig. S16). Likely candidates for other Zfh1 targets are the remaining NSC stemness TFs, such as *ase*, *wor* and *klu*, although direct repression of other stem-cell functions, such as the cell cycle, is also possible.

Other TFs reported to repress NSC genes are Pros (Bayraktar et al., 2010; Cabernard and Doe, 2009; Choksi et al., 2006; Colonques et al., 2011; Liu et al., 2020; Southall and Brand, 2009; Vaessin et al., 1991), LolaN (Flybase: Lola-PP) (Southall et al., 2014) and Nerfin-1 (Froldi et al., 2015; Vissers et al., 2018) in

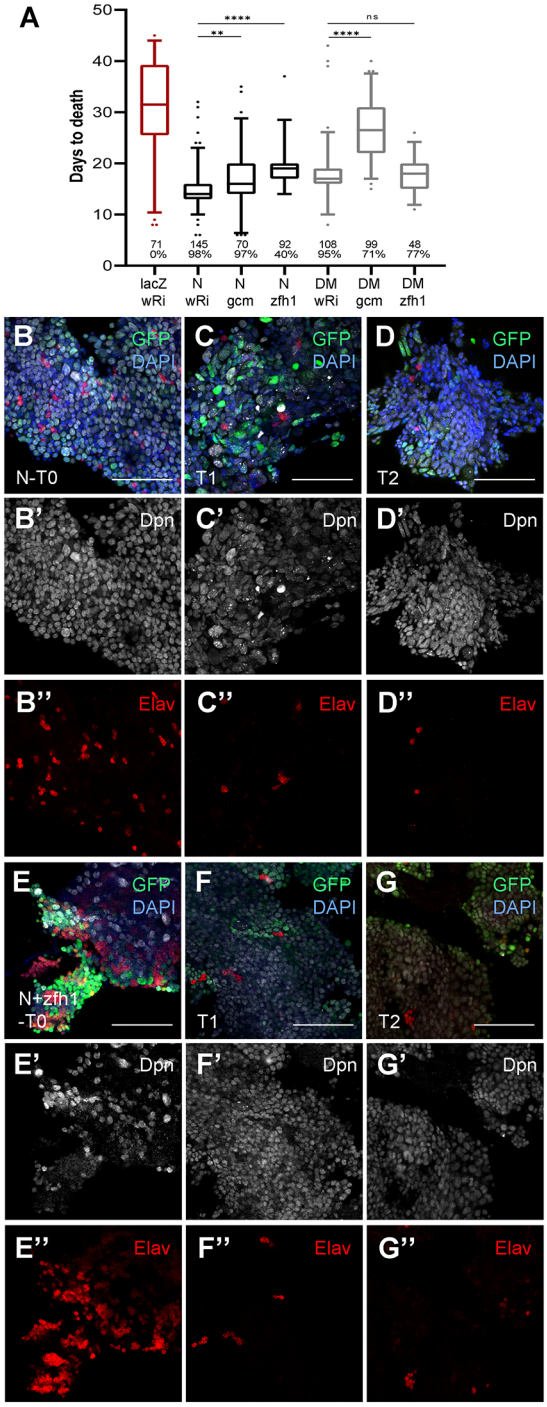

Fig. 10. Effects of *gcm* and *zfh1* misexpression on *N* and *DM* tumorigenesis. (A) Host lifespan after transplantation of larval brain lobes carrying *act>STOP>Gal4* clones of the indicated genotypes; *lacZ* and wRi (white-RNAi) are neutral UAS transgenes. Box-plot: median values (middle bars) and first to third interquartile ranges (boxes); whiskers are 5% and 95%; dots indicate outliers. ***P*<0.01; *****P*<0.0001 (unpaired *t*-test). The percentage of injected flies that developed detectable GFP (under the stereoscope) is shown. In all but the control (*lacZ*+wRi), viability was scored only for GFP-positive flies – numbers of flies scored are shown. (B-G) Progression of *act>N* (B-D) and *act>N+zfh1* (E-G) transplanted tumours. Shown are tumour fragments recovered from the host abdomen and stained for the indicated markers. (B,E) T0 tumour recovered after transplanting larval brain lobe. (C,F) T1 tumour recovered after transplanting T0 tumour pieces. (D,G) T2 tumour recovered after transplanting T1 tumour pieces. Scale bars: 25 µm.

Development (2020) 147, dev191544. doi:10.1242/dev.191544

Type I lineages and Erm in Type II INPs (Janssens et al., 2014; Koe et al., 2014; Weng et al., 2010). All four, like Zfh1, show mutually repressive relationships with the Hes factors: they have strong Dpn binding in their vicinity (Fig. 4) and most are downregulated in *N*/Hes tumours (Fig. 3A, although *pros* downregulation was less than the 1.8× cut-off we imposed). Repression by Hes factors has been reported for *erm* (Janssens et al., 2017; Li et al., 2017) and *pros* (San-Juán and Baonza, 2011; Zhu et al., 2012), and we now show it for *zfh1*. Together Pros, Zfh1, LolaN and Nerfin-1 may therefore constitute a group of TFs that switch off the expression of stemness markers, ensuring their specific accumulation only in the NSCs.

Curiously, these anti-stemness TF genes (*zfh1*, *erm*, *nerfin-1*, *lolaN* and *pros*) are also in the vicinity of experimentally detected Su(H) binding sites, even though Notch activity represses them (Zacharioudaki et al., 2016; this study). Perhaps high Notch signalling in the NSC primes these chromatin regions for activity, but transcription is prevented by the binding of Hes repressors that accumulate to high levels in the NSC. As Notch signalling diminishes in the NSC progeny, Hes proteins disappear and these genes are derepressed. They in turn would serve to repress residual stemness gene transcription in the early-born neurons, in which lower levels of Notch activity are still present, as evidenced by the need for Notch in neuron fate decisions (Truman et al., 2010) and the neuronal expression of *Hey*, another Notch target (Monastirioti et al., 2010).

Do these anti-stemness factors directly promote differentiation, like Gcm? We have evidence that Zfh1 does the contrary, namely antagonizes differentiation. We see this by the loss of early neuronal markers such as Elav upon Zfh1 overexpression (Figs 7 and 8). A plausible scenario is that after GMC divisions, newly-born neurons remain in a developmentally plastic state by virtue of expressing *zfh1* (and probably also *pros*, *lolaN* and *nerfin-1*) and they only differentiate when these factors are downregulated at a later time. When in this plastic state, cells can be reprogrammed by increased Notch/Hes activity leading to ectopic NSCs. In contrast, mature neurons and glia never de-differentiate to NSCs upon the same Notch/Hes stimulation. A similar role in delaying differentiation has been described for Zfh1 and its mammalian homologue ZEB1 during myogenesis (Boukhatmi and Bray, 2018; Siles et al., 2013). We also noted a difference between the activity of Zfh1 and mammalian ZEB1: Whereas ZEB1 is well-known for promoting epithelial-to-mesenchymal transition and enabling tumour progression and metastasis (Brabletz and Brabletz, 2010; Rosmaninho et al., 2018), in our system, Zfh1 suppressed NSC lineage tumorigenesis.

In summary, Notch activity favours NSC fate via setting up a network of TFs that mutually cross-regulate and allow a gradual transition to differentiation as Notch activity dwindles. Why does persistent Notch activity lead to malignant tumours? Our data show that tumorigenesis is not a simple consequence of an inability to differentiate. *N*/*zfh1* and *DM*/*zfh1* CNSs contain more undifferentiated cells than *N* or *DM*, but they are also less tumorigenic. Also, normal NSCs, despite being undifferentiated, do not produce tumours when FACS-sorted and allografted (Landskron et al., 2018). Further studies are needed to characterize the transition of NSC lineages to malignancy.

MATERIALS AND METHODS

DNA constructs

UAS constructs of *dpn*, *E(spl)mγ* and *E(spl)m8* were made by PCR amplifying the coding sequences of these genes (primer sequences are listed in Table S1) from a cDNA template. The cDNA was synthesized from RNA extracted from 30 adult *yw* flies. PCR fragments were subsequently cloned into the pENTR3C entry vector (http://www.ciwemb.edu/labs/murphy/Gateway%20vectors.html) and subsequently N-terminally tagged with 3×HA epitope using the UASt destination vector pTHW by Gateway cloning technology.

These plasmids were injected along with helper plasmid (Δ2–3–transposase) (Karess and Rubin, 1984) into embryos of *yw* to generate transgenic *UAS-HA-dpn*, *UAS-HA-E(spl)mγ* and *UAS-HA-E(spl)m8* flies.

Fly stocks and genetics

Drosophila stocks are described in Flybase and were obtained from the Bloomington *Drosophila* Stock Center (BDSC) unless otherwise indicated. *zfh1-lacZ* is BDSC stock 11515 that carries the *P {PZ}zfh1*^{00865} enhancer trap (Justice et al., 1995; Lai et al., 1991). *gcm-lacZ* is BDSC stock 5445 that carries the *P{PZ}gcm*^{rA87} enhancer trap.

Overproliferating third instar larval CNSs were obtained by crossing *UAS-HA-mγ* and/or *UAS-HA-dpn* flies with *tubP-Gal80ts; UAS-CD8GFP; grhNB-Gal4* (Zacharioudaki et al., 2016). Crosses were maintained at 18°C for 8 days, then transferred to 30°C for 24 h before dissection.

Flip-out clones

Stocks for act flip-out clones were generated as follows: Initially the act-FRT>STOP>FRT-Gal4 (BDSC stock 4780) was recombined with UAS-nlsGFP and subsequently combined with hs-FLP. Flies from the hs-FLP; act-FRT>STOP>FRT-Gal4, UAS-GFP stock were crossed with the appropriate UAS combinations for generating clones. *UAS-zfh1* is BDSC stock 6879 and expresses the long isoform of *zfh1* (RB). *UAS-gcm* was obtained from Fly ORF (Bischof et al., 2013). Control clones were obtained by replacing UAS-lines with *yw*. Progeny underwent heat shock for 45 min-1 h at 37°C at 72 h after egg lay (AEL). Phenotypes were analysed 3 days later, unless otherwise indicated.

For mosaic analysis (MARCM)

FRT82 zfh1$^{75.26}$ (Leatherman and Dinardo, 2008) and *FRTG13 gcm*$^{N7-4}$ (Bernardoni et al., 1997) were crossed to appropriate *FRT tubP-Gal80* counter-chromosomes (Lee and Luo, 1999) combined with *hs-FLP, tubP-Gal4, UAS-GFP* for generating clones. Progeny underwent heat shock for 1 h at 37°C at 72 h AEL and CNSs were dissected out from wandering third instar larvae 3 days post clone induction.

Expression arrays

For each expression array, RNA was isolated from 300 larval CNSs dissected in ice-cold PBS using the RNeasy Plus Mini Kit (Qiagen). Synthesis of double-stranded cDNA and biotin-labelled cRNA was performed according to the manufacturer's instructions (Affymetrix). Fragmented cRNA preparations were hybridized to *Drosophila* genome oligonucleotide arrays [GeneChip *Drosophila* Genome 2.0 Array (3′ IVT Expression Affymetrix)] using an Affymetrix hybridization Oven 640, washed, and then scanned on a GeneChip Scanner 3000.Three replicate arrays were analysed for each genotype. Data from expression arrays have been deposited in Gene Expression Omnibus under accession number GSE141794.

Gene expression values were obtained using Affymetrix Transcription Analysis Console from CEL intensity files using MAS5 without normalization and further quantile-normalized and then filtered for low expression. Differential gene expression analysis was performed on 8479 probesets with detectable expression. For each of the four mutant conditions, $\log_2$-fold-change values were calculated against wt samples, coupled with a Benjamini–Hochberg adjusted *P*-value following an unpaired two-tailed Student's *t*-test.

Differentially expressed genes were defined in the reduced set, based on moderately conservative criteria of absolute $\log_2$(fold-change)≥0.85 (corresponding to fold-change values of >1.8 or <0.55) and corrected *P*-values of ≤0.05 (FDR 5%). The union of all genes differentially expressed in at least one of the studied conditions comprised 1410 genes. These were further clustered in six groups depending on their differential expression across conditions: overexpressed in Notch (114 genes), Hes (417) or both

Development (2020) 147, dev191544. doi:10.1242/dev.191544

Notch and Hes (42), underexpressed in Notch (242), Hes (484), or both Notch and Hes (96). Further comparison of transcriptomes was performed through Pearson correlation calculations of differential expression values for the set of the 1410 inclusive DEGs.

Comparison of differential expression with public datasets was performed through the application of simple thresholds corresponding to the top/bottom 10% of genes being differentially expressed in FACS-sorted neural stem cells versus differentiated neurons (Berger et al., 2012). Differential expression values in the four studied conditions were then analysed for sets of ∼1600 genes corresponding to neuron and neuroblast-specific expression, respectively (Fig. S8). To compare our CNS transcriptomes with those of other CNS tumours, we obtained data for *l(3)mbt* (Janic et al., 2010), *l(2)gl*, *scrib* (Richardson lab, GEO: GSE48852) and two *brat* RNAi genotypes (Neumüller et al., 2011), and cross-analysed gene expression levels for our restricted 1410 DEGs (Fig. S9), and against the extended set of 8479 measured genes (Fig. 3D). This comparison was performed at the level of differential expression, which largely removes biases owing to genotypic variation, experimental procedures and processing, as all values refer to wt controls. Log(fold-change) data, being relative values, represent the best way for cross comparison of gene expression profiles. Clustering of gene expression profiles was performed on the basis of Spearman Rank Correlation for all 8479 genes. Spearman rank was preferred to linear measures (such as Pearson correlation coefficient), as our focus was on monitoring monotonic relationships between tumours that were unlikely to be linear owing to the inherent variability of the samples (coming from different experiments).

We used PANTHER (http://www.pantherdb.org/) (Mi et al., 2019) to assess statistical overrepresentation. Genes were provided as lists of Flybase FBgn IDs (Thurmond et al., 2019) to PANTHER and analysed at the levels of GO (Biological Process and Molecular Function). An adjusted *P*-value of ≤0.05 was set as the threshold for significance.

qPCR

Larval CNSs of different genotypes were dissected and kept in Trizol, where they were homogenized with a plastic pestle and incubated for 10 min on ice. RNA was extracted using chloroform and precipitated in isopropanol overnight at −20°C. RNA was resuspended in RNase-free water and subsequently treated with DNA-free™ DNase (Invitrogen, now Thermo Fisher Scientific, AM1906) for removal of genomic DNA. Then 700 ng of RNA was reverse transcribed with oligo$(dT)_{15}$ primers (Promega C1101) using SuperScript III Reverse Transcriptase (Invitrogen, now Thermo Fisher Scientific, 18080044). The cDNA products were subsequently diluted 1:5 and 2 µl were used as a template in each qPCR reaction. qPCR was performed using KAPA SYBR Green fast Master PCR Kit (Roche, SFUKB-KK, 04707516001). Generation of specific PCR products was confirmed by melting-curve analysis. Ct values for all genes were normalized to the levels of *GAPDH*. For data analysis, the delta-delta Ct values was applied. Primer sequences are listed in Table S2.

ChIP

For each ChIP analysis, chromatin was prepared from 500 third instar larval CNSs dissected from the cross *grhNB-Gal4×UAS-myγ; UAS-dpn*. Tissues were cross-linked with 1% formaldehyde, quenched with 200 mM glycine. After homogenization in Nuclear Lysis Buffer [50 mM Tris-HCl (pH 8), 10 mM EDTA, 1% SDS and protease inhibitor], chromatin was fragmented using Diagenode Bioruptor for 7 cycles with 30 s OFF/30 s ON to obtain 200-500 bp length. Fragmented chromatin was immunoprecipitated with anti-Dpn antibody (see Supplementary Materials and Methods for production method) overnight at 4°C. Complexes were incubated with Protein A/G agarose beads (SC-2003) and precipitated chromatin was eluted using IP Elution Buffer (100 mM $NaHC0_3$, 1% SDS) and purified using Qiagen PCR purification kit. Validation of enrichment was performed over specific chromatin regions (Primer sequences in Table S3).

Ion Torrent library sequencing and data processing

Two biological replicates of anti-Dpn ChIP and one input were sequenced on an Ion Torrent Proton platform with Ion 540 ChIP kits (Thermo Fisher Scientific, #A27765). Libraries were prepared according to manufacturer's protocol using the Ion Plus Library Kit (Thermo Fisher Scientific, #4471252).

Fastq reads were mapped to University of California, Santa Cruz (UCSC)/dm3 genome (archive-2015-07-17-14-30-40) downloaded from iGenomes using bowtie2 (version 2.2.8, –very-sensitive) (Langmead and Salzberg, 2012). Bedgraphs of mapped reads were generated by bedtools genomecov (v2.25.0) and uploaded on UCSC/Berkeley *Drosophila* Genome Project R5/dm3 genome browser for visualization. Reads that overlapped with dm3 repeat elements (downloaded from UCSC) were removed from bam files before peak calling using bamtools intersect (default). Peak calling was performed with macs2 over input (-p 0.05, version 2.1.0.20140616) (Zhang et al., 2008). A Dpn binding consensus list of 229 genomic regions was generated using peaks with fold-change>2 over input in both biological replicates. Motif enrichment analysis was performed in cistrome (Liu et al., 2011) using the SeqPos motif tool, searching against known *Drosophila melanogaster* transcription factor binding motifs from Jaspar. Genome wide peak distribution was performed with the pavis tool (Huang et al., 2013) using the Flybase R5.57/dm3 genome assembly and a 5kb upstream and 5kb downstream length window. Peak to gene annotation was performed by bedtools intersect using the Dpn binding consensus and the RefseqFlat.txt with 5kb upstream and 5kb downstream window extensions for each Refseq transcript. Gene ontology analysis of the genes with peaks in their proximity was performed using flymine v47.1 (Lyne et al., 2007). ChIP data have been deposited in Gene Expression Omnibus (GSE141794).

Immunohistochemistry

Fixation and immunohistochemistry of larval tissues were performed according to standard protocols (Daskalaki et al., 2011). Details of primary and secondary antibodies are provided in Tables S4 and S5. Samples were imaged on a Leica SP8 confocal microscope at the Confocal Facility, Institute of Molecular Biology and Biotechnology (IMBB) of the Foundation for Research and Technology Hellas (FORTH).

Transplantation assay

Transplantation assays were performed as previously described by Rossi and Gonzalez (2015). Donor larval brains were made using FLP-out GFP clones or a *tubGal80ts grhNB-Gal4 UAS-stinger-RFP* combination to overexpress different transgene combinations. CNSs were dissected, sliced into single brain lobes or single VNCs, loaded into a fine glass needle and implanted into the abdomen of female host w1118 flies using a nanoinjector (Nanoject II Auto-Nanoliter Injector, Drummond Scientific Company, 3-000-205A). Host flies carrying allografts were kept at 25°C (GFP allografts) or 30°C (RFP allografts) and examined daily for viability and the presence of GFP/RFP in their abdomen and other tissues. Malignant GFP/RFP-positive tumour pieces (T0) were dissected out of the abdomen of host flies and either re-transplanted into new host flies (T1) or fixed with 4% formaldehyde (for 25 min at room temperature) and used for immunohistochemistry experiments according to standard protocols (Daskalaki et al., 2011). Alternatively they were stored in Trizol for RNA extraction and qRT-PCR.

Acknowledgements

We are grateful to Sarah J. Bray and Cayetano Gonzalez for hosting S.S.M. and training him in chromatin immunoprecipitation and tumour allografting. We thank Ioannis Livadaras and Alexandros Babaratsas for fly injections and maintenance. Microarray hybridizations and high-throughput sequencing were performed at the IMBB genomics facility. Many thanks to Erika Bach, Stephen DiNardo, Angela Giangrande, Yuh Nung Jan, Ruth Lehmann, James Skeath and Isabel Guerrero for providing fly stocks and antibodies.

Competing interests

The authors declare no competing or financial interests.

Author contributions

Conceptualization: S.S.M., C.D.; Methodology: S.S.M., C.D.; Validation: S.S.M., G.A., E.Z.; Formal analysis: V.T., C.N.; Investigation: S.S.M., C.V., G.A., E.Z., I.K.P.,

C.E., M.S., K.A.K., J.F.F., C.D.; Resources: S.S.M.; Data curation: S.S.M., V.T., C.N.; Writing - original draft: C.D.; Writing - review & editing: C.D.; Visualization: S.S.M., E.Z., C.D.; Supervision: C.D.; Project administration: C.D.; Funding acquisition: C.D.

Funding
Funding for this work was provided by the H2020 Marie Skłodowska-Curie Actions HEALING (ITN consortium), a Worldwide Cancer Research grant to C.D., a Fondation Santé grant to C.D., a Hellenic Foundation for Research & Innovation grant to E.Z. and two short- term grants, from EMBO and The Company of Biologists, to S.S.M.

Data availability
Data from expression arrays have been deposited in Gene Expression Omnibus under accession number GSE141794.

Supplementary information
Supplementary information available online at
https://dev.biologists.org/lookup/doi/10.1242/dev.191544.supplemental

Peer review history
The peer review history is available online at
https://dev.biologists.org/lookup/doi/10.1242/dev.191544.reviewer-comments.pdf

References
Almeida, M. S. and Bray, S. J. (2005). Regulation of post-embryonic neuroblasts by *Drosophila* grainyhead. *Mech. Dev.* **122**, 1282-1293. doi:10.1016/j.mod.2005.08.004

Awasaki, T., Lai, S.-L., Ito, K. and Lee, T. (2008). Organization and postembryonic development of glial cells in the adult central brain of *Drosophila*. *J. Neurosci.* **28**, 13742-13753. doi:10.1523/JNEUROSCI.4844-08.2008

Baumgardt, M., Karlsson, D., Salmani, B. Y., Bivik, C., MacDonald, R. B., Gunnar, E. and Thor, S. (2014). Global programmed switch in neural daughter cell proliferation mode triggered by a temporal gene cascade. *Dev. Cell* **30**, 192-208. doi:10.1016/j.devcel.2014.06.021

Bayraktar, O. A., Boone, J. Q., Drummond, M. L. and Doe, C. Q. (2010). Drosophila type II neuroblast lineages keep prospero levels low to generate large clones that contribute to the adult brain central complex. *Neural Dev.* **5**, 26. doi:10.1186/1749-8104-5-26

Beaucher, M., Goodliffe, J., Hersperger, E., Trunova, S., Frydman, H. and Shearn, A. (2007). Drosophila brain tumor metastases express both neuronal and glial cell type markers. *Dev. Biol.* **301**, 287-297. doi:10.1016/j.ydbio.2006.09.019

Berger, C., Harzer, H., Burkard, T. R., Steinmann, J., van der Horst, S., Laurenson, A.-S., Novatchkova, M., Reichert, H. and Knoblich, J. A. (2012). FACS purification and transcriptome analysis of drosophila neural stem cells reveals a role for Klumpfuss in self-renewal. *Cell Rep.* **2**, 407-418. doi:10.1016/j.celrep.2012.07.008

Bernardoni, R., Vivancos, V. and Giangrande, A. (1997). glide/gcm is expressed and required in the scavenger cell lineage. *Dev. Biol.* **191**, 118-130. doi:10.1006/dbio.1997.8702

Bier, E., Vaessin, H., Younger-Shepherd, S., Jan, L. Y. and Jan, Y. N. (1992). deadpan, an essential pan-neural gene in Drosophila, encodes a helix-loop-helix protein similar to the hairy gene product. *Genes Dev.* **6**, 2137-2151. doi:10.1101/gad.6.11.2137

Bischof, J., Bjorklund, M., Furger, E., Schertel, C., Taipale, J. and Basler, K. (2013). A versatile platform for creating a comprehensive UAS-ORFeome library in Drosophila. *Development* **140**, 2434-2442. doi:10.1242/dev.088757

Boukhatmi, H. and Bray, S. (2018). A population of adult satellite-like cells in Drosophila is maintained through a switch in RNA-isoforms. *eLife* **7**, e35954. doi:10.7554/eLife.35954

Bowman, S. K., Rolland, V., Betschinger, J., Kinsey, K. A., Emery, G. and Knoblich, J. A. (2008). The tumor suppressors brat and numb regulate transit-amplifying neuroblast lineages in Drosophila. *Dev. Cell* **14**, 535-546. doi:10.1016/j.devcel.2008.03.004

Brabletz, S. and Brabletz, T. (2010). The ZEB/miR-200 feedback loop—a motor of cellular plasticity in development and cancer? *EMBO Rep.* **11**, 670-677. doi:10.1038/embor.2010.117

Cabernard, C. and Doe, C. Q. (2009). Apical/basal spindle orientation is required for neuroblast homeostasis and neuronal differentiation in Drosophila. *Dev. Cell* **17**, 134-141. doi:10.1016/j.devcel.2009.06.009

Cattenoz, P. B., Popkova, A., Southall, T. D., Aiello, G., Brand, A. H. and Giangrande, A. (2016). Functional conservation of the glide/Gcm regulatory network controlling glia, hemocyte, and tendon cell differentiation in Drosophila. *Genetics* **202**, 191-219. doi:10.1534/genetics.115.182154

Caussinus, E. and Gonzalez, C. (2005). Induction of tumor growth by altered stem-cell asymmetric division in Drosophila melanogaster. *Nat. Genet.* **37**, 1125-1129. doi:10.1038/ng1632

Choksi, S. P., Southall, T. D., Bossing, T., Edoff, K., de Wit, E., Fischer, B. E., van Steensel, B., Micklem, G. and Brand, A. H. (2006). Prospero acts as a binary switch between self-renewal and differentiation in Drosophila neural stem cells. *Dev. Cell* **11**, 775-789. doi:10.1016/j.devcel.2006.09.015

Colonques, J., Ceron, J., Reichert, H. and Tejedor, F. J. (2011). A transient expression of prospero promotes cell cycle exit of Drosophila postembryonic neurons through the regulation of dacapo. *PLoS ONE* **6**, e19342. doi:10.1371/journal.pone.0019342

Daskalaki, A., Shalaby, N. A., Kux, K., Tsoumpekos, G., Tsibidis, G. D., Muskavitch, M. A. T. and Delidakis, C. (2011) Distinct intracellular motifs of Delta mediate its ubiquitylation and activation by Mindbomb1 and Neuralized. *J. Cell Biol.* **195**, 1017-1031. doi:10.1083/jcb.201105166

Enriquez, J., Venkatasubramanian, L., Baek, M., Peterson, M., Aghayeva, U. and Mann, R. S. (2015). Specification of individual adult motor neuron morphologies by combinatorial transcription factor codes. *Neuron* **86**, 955-970. doi:10.1016/j.neuron.2015.04.011

Froldi, F., Szuperak, M., Weng, C.-F., Shi, W., Papenfuss, A. T. and Cheng, L. Y. (2015). The transcription factor Nerfin-1 prevents reversion of neurons into neural stem cells. *Genes Dev.* **29**, 129-143. doi:10.1101/gad.250282.114

Gateff, E. (1978). Malignant neoplasms of genetic origin in Drosophila melanogaster. *Science* **200**, 1448-1459. doi:10.1126/science.96525

Homem, C. C. F., Repic, M. and Knoblich, J. A. (2015). Proliferation control in neural stem and progenitor cells. *Nat. Rev. Neurosci.* **16**, 647-659. doi:10.1038/nrn4021

Huang, W., Loganantharaj, R., Schroeder, B., Fargo, D. and Li, L. (2013). PAVIS: a tool for peak annotation and visualization. *Bioinformatics* **29**, 3097-3099. doi:10.1093/bioinformatics/btt520

Janic, A., Mendizabal, L., Llamazares, S., Rossell, D. and Gonzalez, C. (2010). Ectopic expression of germline genes drives malignant brain tumor growth in Drosophila. *Science* **330**, 1824-1827. doi:10.1126/science.1195481

Janssens, D. H., Komori, H., Grbac, D., Chen, K., Koe, C. T., Wang, H. and Lee, C.-Y. (2014). Earmuff restricts progenitor cell potential by attenuating the competence to respond to self-renewal factors. *Development* **141**, 1036-1046. doi:10.1242/dev.106534

Janssens, D. H., Hamm, D. C., Anhezini, L., Xiao, Q., Siller, K. H., Siegrist, S. E., Harrison, M. M. and Lee, C.-Y. (2017). An Hdac1/Rpd3-poised circuit balances continual self-renewal and rapid restriction of developmental potential during asymmetric stem cell division. *Dev. Cell* **40**, 367-380.e7. doi:10.1016/j.devcel.2017.01.014

Jennings, B. H., Tyler, D. M. and Bray, S. J. (1999). Target specificities of Drosophila enhancer of split basic helix-loop-helix proteins. *Mol. Cell Biol.* **19**, 4600-4610. doi:10.1128/MCB.19.7.4600

Jones, B. W., Fetter, R. D., Tear, G. and Goodman, C. S. (1995). glial cells missing: a genetic switch that controls glial versus neuronal fate. *Cell* **82**, 1013-1023. doi:10.1016/0092-8674(95)90280-5

Justice, R. W., Zilian, O., Woods, D. F., Noll, M. and Bryant, P. J. (1995). The Drosophila tumor suppressor gene warts encodes a homolog of human myotonic dystrophy kinase and is required for the control of cell shape and proliferation. *Genes Dev.* **9**, 534-546. doi:10.1101/gad.9.5.534

Kageyama, R., Shimojo, H. and Ohtsuka, T. (2019). Dynamic control of neural stem cells by bHLH factors. *Neurosci. Res.* **138**, 12-18. doi:10.1016/j.neures.2018.09.005

Kang, K. H. and Reichert, H. (2015). Control of neural stem cell self-renewal and differentiation in Drosophila. *Cell Tissue Res.* **359**, 33-45. doi:10.1007/s00441-014-1914-9

Karess, R. E. and Rubin, G. M. (1984). Analysis of P transposable element functions in Drosophila. *Cell* **38**, 135-146. doi:10.1016/0092-8674(84)90534-8

Knoblich, J. A., Jan, L. Y. and Jan, Y. N. (1995). Asymmetric segregation of numb and prospero during cell division. *Nature* **377**, 624-627. doi:10.1038/377624a0

Koe, C. T., Li, S., Rossi, F., Wong, J. J. L., Wang, Y., Zhang, Z., Chen, K., Aw, S. S., Richardson, H. E., Robson, P. et al. (2014). The Brm-HDAC3-Erm repressor complex suppresses dedifferentiation in Drosophila type II neuroblast lineages. *eLife* **3**, e01906. doi:10.7554/eLife.01906

Koumbanakis, K. (2007). In vitro και in vivo μελέτες της πρόσδεσης των πρωτεϊνών bHLH E(spl) σε στόχους DNA. [In vitro and in vivo studies of E(spl)bHLH protein binding to DNA targets]: Department of Biology, University of Crete, Greece.

Lai, Z., Fortini, M. E. and Rubin, G. M. (1991). The embryonic expression patterns of zfh-1 and zfh-2, two Drosophila genes encoding novel zinc-finger homeodomain proteins. *Mech. Dev.* **34**, 123-134. doi:10.1016/0925-4773(91)90049-C

Landskron, L., Steinmann, V., Bonnay, F., Burkard, T. R., Steinmann, J., Reichardt, I., Harzer, H., Laurenson, A.-S., Reichert, H., Knoblich, J. A. et al. (2018). The asymmetrically segregating lncRNA cherub is required for transforming stem cells into malignant cells. *eLife* **7**, e31347. doi:10.7554/eLife.31347

Langmead, B. and Salzberg, S. L. (2012). Fast gapped-read alignment with bowtie 2. *Nat. Methods* **9**, 357-359. doi:10.1038/nmeth.1923

Layden, M. J., Odden, J. P., Schmid, A., Garces, A., Thor, S. and Doe, C. Q. (2006). Zfh1, a somatic motor neuron transcription factor, regulates axon exit from the CNS. *Dev. Biol.* **291**, 253-263. doi:10.1016/j.ydbio.2005.12.009

Leatherman, J. L. and Dinardo, S. (2008). Zfh-1 controls somatic stem cell self-renewal in the Drosophila testis and nonautonomously influences germline stem cell self-renewal. *Cell Stem Cell* **3**, 44-54. doi:10.1016/j.stem.2008.05.001
Lee, T. (2017). Wiring the Drosophila brain with individually tailored neural lineages. *Curr. Biol.* **27**, R77-R82. doi:10.1016/j.cub.2016.12.026
Lee, T. and Luo, L. (1999). Mosaic analysis with a repressible cell marker for studies of gene function in neuronal morphogenesis. *Neuron* **22**, 451-461. doi:10.1016/S0896-6273(00)80701-1
Li, X., Erclik, T., Bertet, C., Chen, Z., Voutev, R., Venkatesh, S., Morante, J., Celik, A. and Desplan, C. (2013). Temporal patterning of Drosophila medulla neuroblasts controls neural fates. *Nature* **498**, 456-462. doi:10.1038/nature12319
Li, X., Chen, R. and Zhu, S. (2017). bHLH-O proteins balance the self-renewal and differentiation of Drosophila neural stem cells by regulating Earmuff expression. *Dev. Biol.* **431**, 239-251. doi:10.1016/j.ydbio.2017.09.011
Lin, S., Lai, S.-L., Yu, H.-H., Chihara, T., Luo, L. and Lee, T. (2010). Lineage-specific effects of notch/numb signaling in post-embryonic development of the Drosophila brain. *Development* **137**, 43-51. doi:10.1242/dev.041699
Liu, T., Ortiz, J. A., Taing, L., Meyer, C. A., Lee, B., Zhang, Y., Shin, H., Wong, S. S., Ma, J., Lei, Y. et al. (2011). Cistrome: an integrative platform for transcriptional regulation studies. *Genome Biol.* **12**, R83. doi:10.1186/gb-2011-12-8-r83
Liu, X., Shen, J., Xie, L., Wei, Z., Wong, C., Li, Y., Zheng, X., Li, P. and Song, Y. (2020). Mitotic implantation of the transcription factor prospero via phase separation drives terminal neuronal differentiation. *Dev. Cell* **52**, 277-293.e8. doi:10.1016/j.devcel.2019.11.019
Loedige, I., Jakob, L., Treiber, T., Ray, D., Stotz, M., Treiber, N., Hennig, J., Cook, K. B., Morris, Q., Hughes, T. R. et al. (2015). The crystal structure of the NHL domain in complex with rna reveals the molecular basis of drosophila brain-tumor-mediated gene regulation. *Cell Rep.* **13**, 1206-1220. doi:10.1016/j.celrep.2015.09.068
Lyne, R., Smith, R., Rutherford, K., Wakeling, M., Varley, A., Guillier, F., Janssens, H., Ji, W., McLaren, P., North, P. et al. (2007). FlyMine: an integrated database for Drosophila and anopheles genomics. *Genome Biol.* **8**, R129. doi:10.1186/gb-2007-8-7-r129
Maurange, C., Cheng, L. and Gould, A. P. (2008). Temporal transcription factors and their targets schedule the end of neural proliferation in Drosophila. *Cell* **133**, 891-902. doi:10.1016/j.cell.2008.03.034
Mi, H., Muruganujan, A., Ebert, D., Huang, X. and Thomas, P. D. (2019). PANTHER version 14: more genomes, a new PANTHER GO-slim and improvements in enrichment analysis tools. *Nucleic Acids Res.* **47**, D419-D426. doi:10.1093/nar/gky1038
Monastirioti, M., Giagtzoglou, N., Koumbanakis, K. A., Zacharioudaki, E., Deligiannaki, M., Wech, I., Almeida, M., Preiss, A., Bray, S. and Delidakis, C. (2010). Drosophila hey is a target of notch in asymmetric divisions during embryonic and larval neurogenesis. *Development* **137**, 191-201. doi:10.1242/dev.043604
Narbonne-Reveau, K., Lanet, E., Dillard, C., Foppolo, S., Chen, C.-H., Parrinello, H., Rialle, S., Sokol, N. S. and Maurange, C. (2016). Neural stem cell-encoded temporal patterning delineates an early window of malignant susceptibility in *Drosophila*. *eLife* **5**, e13463. doi:10.7554/eLife.13463
Neumüller, R. A., Richter, C., Fischer, A., Novatchkova, M., Neumüller, K. G. and Knoblich, J. A. (2011). Genome-wide analysis of self-renewal in Drosophila neural stem cells by transgenic RNAi. *Cell Stem Cell* **8**, 580-593. doi:10.1016/j.stem.2011.02.022
Paridaen, J. T. M. L. and Huttner, W. B. (2014). Neurogenesis during development of the vertebrate central nervous system. *EMBO Rep.* **15**, 351-364. doi:10.1002/embr.201438447
Postigo, A. A., Ward, E., Skeath, J. B. and Dean, D. C. (1999). zfh-1, the Drosophila homologue of ZEB, is a transcriptional repressor that regulates somatic myogenesis. *Mol. Cell Biol.* **19**, 7255-7263. doi:10.1128/MCB.19.10.7255
Ragone, G., Van De Bor, V., Sorrentino, S., Kammerer, M., Galy, A., Schenck, A., Bernardoni, R., Miller, A. A., Roy, N. and Giangrande, A. (2003). Transcriptional regulation of glial cell specification. *Dev. Biol.* **255**, 138-150. doi:10.1016/S0012-1606(02)00081-7
Reichardt, I., Bonnay, F., Steinmann, V., Loedige, I., Burkard, T. R., Meister, G. and Knoblich, J. A. (2018). The tumor suppressor brat controls neuronal stem cell lineages by inhibiting deadpan and zelda. *EMBO Rep.* **19**, 102-117. doi:10.15252/embr.201744188
Richter, C., Oktaba, K., Steinmann, J., Müller, J. and Knoblich, J. A. (2011). The tumour suppressor L(3)mbt inhibits neuroepithelial proliferation and acts on insulator elements. *Nat. Cell Biol.* **13**, 1029-1039. doi:10.1038/ncb2306
Rosmaninho, P., Mükusch, S., Piscopo, V., Teixeira, V., Raposo, A. A. S. F., Warta, R., Bennewitz, R., Tang, Y., Herold-Mende, C., Stifani, S. et al. (2018). Zeb1 potentiates genome-wide gene transcription with Lef1 to promote glioblastoma cell invasion. *EMBO J.* **37**, e97115. doi:10.15252/embj.201797115
Rossi, F. and Gonzalez, C. (2015). Studying tumor growth in Drosophila using the tissue allograft method. *Nat. Protoc.* **10**, 1525-1534. doi:10.1038/nprot.2015.096
San-Juán, B. P. and Baonza, A. (2011). The bHLH factor deadpan is a direct target of notch signaling and regulates neuroblast self-renewal in Drosophila. *Dev. Biol.* **352**, 70-82. doi:10.1016/j.ydbio.2011.01.019
Sellin, J., Drechsler, M., Nguyen, H. T. and Paululat, A. (2009). Antagonistic function of Lmd and Zfh1 fine tunes cell fate decisions in the Twi and Tin positive mesoderm of Drosophila melanogaster. *Dev. Biol.* **326**, 444-455. doi:10.1016/j.ydbio.2008.10.041
Siles, L., Sanchez-Tillo, E., Lim, J.-W., Darling, D. S., Kroll, K. L. and Postigo, A. (2013). ZEB1 imposes a temporary stage-dependent inhibition of muscle gene expression and differentiation via CtBP-mediated transcriptional repression. *Mol. Cell. Biol.* **33**, 1368-1382. doi:10.1128/MCB.01259-12
Sousa-Nunes, R., Cheng, L. Y. and Gould, A. P. (2010). Regulating neural proliferation in the Drosophila CNS. *Curr. Opin. Neurobiol.* **20**, 50-57. doi:10.1016/j.conb.2009.12.005
Soustelle, L. and Giangrande, A. (2007). Novel gcm-dependent lineages in the postembryonic nervous system of Drosophila melanogaster. *Dev. Dyn.* **236**, 2101-2108. doi:10.1002/d vdy.21232
Southall, T. D. and Brand, A. H. (2009). Neural stem cell transcriptional networks highlight genes essential for nervous system development. *EMBO J.* **28**, 3799-3807. doi:10.1038/emboj.2009.309
Southall, T. D., Davidson, C. M., Miller, C., Carr, A. and Brand, A. H. (2014). Dedifferentiation of neurons precedes tumor formation in Lola mutants. *Dev. Cell* **28**, 685-696. doi:10.1016/j.devcel.2014.01.030
Spana, E. P. and Doe, C. Q. (1996). Numb antagonizes Notch signaling to specify sibling neuron cell fates. *Neuron* **17**, 21-26. doi:10.1016/S0896-6273(00)80277-9
Thurmond, J., Goodman, J. L., Strelets, V. B., Attrill, H., Gramates, L. S., Marygold, S. J., Matthews, B. B., Millburn, G., Antonazzo, G., Trovisco, V. et al. (2019). FlyBase 2.0: the next generation. *Nucleic Acids Res.* **47**, D759-D765. doi:10.1093/nar/gky1003
Truman, J. W., Moats, W., Altman, J., Marin, E. C. and Williams, D. W. (2010). Role of Notch signaling in establishing the hemilineages of secondary neurons in Drosophila melanogaster. *Development* **137**, 53-61. doi:10.1242/dev.041749
Vaessin, H., Grell, E., Wolff, E., Bier, E., Jan, L. Y. and Jan, Y. N. (1991). *prospero* is expressed in neuronal precursors and encodes a nuclear protein that is involved in the control of axonal outgrowth in Drosophila. *Cell* **67**, 941-953. doi:10.1016/0092-8674(91)90367-8
Viktorin, G., Riebli, N., Popkova, A., Giangrande, A. and Reichert, H. (2011). Multipotent neural stem cells generate glial cells of the central complex through transit amplifying intermediate progenitors in Drosophila brain development. *Dev. Biol.* **356**, 553-565. doi:10.1016/j.ydbio.2011.06.013
Viktorin, G., Riebli, N. and Reichert, H. (2013). A multipotent transit-amplifying neuroblast lineage in the central brain gives rise to optic lobe glial cells in Drosophila. *Dev. Biol.* **379**, 182-194. doi:10.1016/j.ydbio.2013.04.020
Vissers, J. H. A., Froldi, F., Schröder, J., Papenfuss, A. T., Cheng, L. Y. and Harvey, K. F. (2018). The scalloped and Nerfin-1 transcription factors cooperate to maintain neuronal cell fate. *Cell Rep.* **25**, 1561-1576.e7. doi:10.1016/j.celrep.2018.10.038
Wang, H., Somers, G. W., Bashirullah, A., Heberlein, U., Yu, F. and Chia, W. (2006). Aurora-A acts as a tumor suppressor and regulates self-renewal of Drosophila neuroblasts. *Genes Dev.* **20**, 3453-3463. doi:10.1101/gad.1487506
Weng, M., Golden, K. L. and Lee, C.-Y. (2010). dFezf/Earmuff maintains the restricted developmental potential of intermediate neural progenitors in Drosophila. *Dev. Cell* **18**, 126-135. doi:10.1016/j.devcel.2009.12.007
Winston, R. L., Millar, D. P., Gottesfeld, J. M. and Kent, S. B. H. (1999). Characterization of the DNA binding properties of the bHLH domain of deadpan to single and tandem sites. *Biochemistry* **38**, 5138-5146. doi:10.1021/bi982856a
Wissel, S., Harzer, H., Bonnay, F., Burkard, T. R., Neümuller, R. A. and Knoblich, J. A. (2018). Time-resolved transcriptomics in neural stem cells identifies a v-ATPase/Notch regulatory loop. *J. Cell Biol.* **217**, 3285-3300. doi:10.1083/jcb.201711167
Zacharioudaki, E., Magadi, S. S. and Delidakis, C. (2012). bHLH-O proteins are crucial for Drosophila neuroblast self-renewal and mediate Notch-induced overproliferation. *Development* **139**, 1258-1269. doi:10.1242/dev.071779
Zacharioudaki, E., Housden, B. E., Garinis, G., Stojnic, R., Delidakis, C. and Bray, S. J. (2016). Genes implicated in stem cell identity and temporal programme are directly targeted by notch in neuroblast tumours. *Development* **143**, 219-231. doi:10.1242/dev.126326
Zacharioudaki, E., Falo Sanjuan, J. and Bray, S. (2019). Mi-2/NuRD complex protects stem cell progeny from mitogenic Notch signaling. *eLife* **8**, e41637. doi:10.7554/eLife.41637
Zhang, Y., Liu, T., Meyer, C. A., Eeckhoute, J., Johnson, D. S., Bernstein, B. E., Nusbaum, C., Myers, R. M., Brown, M., Li, W. et al. (2008). Model-based analysis of ChIP-Seq (MACS). *Genome Biol.* **9**, R137. doi:10.1186/gb-2008-9-9-r137
Zhu, S., Wildonger, J., Barshow, S., Younger, S., Huang, Y. and Lee, T. (2012). The bHLH repressor deadpan regulates the self-renewal and specification of Drosophila larval neural stem cells independently of Notch. *PLOS ONE* **7**, e46724. doi:10.1371/journal.pone.0046724

Supplementary Materials and Methods

Table S1: Primers list - cloning

Primer Name	Primer FOR sequence	Primer REV Sequence
dpn	CCGGAATTCATGGATTACAAAAACG	ATCTCGAGCTACCACGGCCTCCAAG
mγ	CGGGATCCATGTCGTCGCTACAAATGTC	CGGAATTCCTACCAGGGACGCCAGAC
m8	CGGGATCCATGGAATACACCACCAAGAC	CGGAATTCTTACCAGGGGCGCCACAAG

Table S2: Primers list - qRT-PCR

Primer Name	Primer FOR sequence	Primer REV Sequence
dpn	TCAACGAACTGAAGTCCCTTATCC	GAATCCCGTCTTGAACTTCTGG
earmuff	AGGATCAGGGCGAAGTGACG	GTGGGCGTTGAACACCTTGC
gcm	TTTCCGCATCTCACCAATTA	ATATGTCGCGTCCATTTGAA
miranda	AGATCAACGAGCTCCTGTCC	CAGTCTTCTTGGGAGTGCTG
nerfin-1	ATGCCAGGGAGAACTACGAC	AATCTGAAGCCGTCCGTATC
Rpl32 (rp49)	AGCATACAGGCCCAAGATCG	GCACCAGGAACTTCTTGAATCC
Gapdh	TTCGCTGAACGATAAGTTCG	ACTTGATCAGGTCGATGACG

Table S3: Primers list - ChIP

Primer Name	Primer FOR sequence	Primer REV Sequence
gcmE1	ATAGGGAACTGGGAGCTGGGAG	ATCGAGTGCCTCAAACCCCTG
gcmE2	TCTGCCAAGGAGTCGCCCAAAG	CAGGTAGGATGTGCTTCCCCAG
gcmE3	ACATTCCAATGGCCCCAGGATTG	TCAGAAGCCGTCGATCTCCTTTC
zfh1E1	ATTTCTCCGCTCGCGAGTCCTG	TGAACGCTCGCCGAAAAAGCAC
zfh1E2	TCCCTCGATAGTTCAGGTAAACCG	AGCAGCTGGAAAAGGTCCTTG
zfh1E3	ACGACCAATGTGCGCACCTTG	AGAGAGAGATAGCCGCCGGAGAG
erm	GTGTGCCGATCATCCTGTTC	GACGATTTCGCTTTCGTTGC

Deadpan antibody production

Dpn ORF cloned in pET29a vector was a gift from James Skeath (Skeath et al., 2017). Protein production was performed according to Novagen manual for protein expression. Ni-NTA beads (Qiagen cat# 30210) purified protein was run on SDS-PAGE, the protein bands were excised and sent to Davids biotechnologie for guinea-pig immunization. The serum obtained caprylic acid treated, dialysed against 1x PBS and aliquots were stored at -80°C.

Table S4: List of 1° antibodies

Antibody (dilution)	Origin
Guinea pig a-Dpn (1:2000)	Made in this study
Guinea pig a-Ase (1:1000)	(Bhalerao et al., 2005)
Rabbit a-Ase (1:1000)	(Brand et al., 1993)
Mouse a-Pros (1:50)	DSHB, MR1A (C. Q. Doe)
Rabbit a-PH3 (1:2000)	Millipore/Sigma-Aldrich, 06-570
Rabbit a-GFP (1:10000)	Minotech, 701-1
Mouse a-GFP (1:100)	DSHB, GFP-G1 (J. R. Sanes/M. Yamagata)
Rat a-Elav (1:300)	DSHB, 7E8A10 (G. M. Rubin)
Mouse a-Repo (1:50)	DSHB, 8D12 (C. Goodman)
Rabbit a-Mira (1:1000)	(Caussinus and Gonzalez, 2005)
Rabbit a-β-Galactosidase (1:10000)	Cappel, 55976 (discontinued)

The monoclonal antibodies marked "DSHB" were obtained from the Developmental Studies Hybridoma Bank, created by the NICHD of the NIH and maintained at The University of Iowa, Department of Biology, Iowa City, IA 52242; in parenthesis we list the investigator who developed each mAb.

Table S5: List of 2° antibodies

Antibody (dilution)	**Origin**
Alexa405-goat anti-rabbit (1:2000)	Life Biotech. (Mol. Probes), A31556
Alexa488-donkey anti-rabbit (1:2000)	Life Biotech. (Mol. Probes), A21206
Cy3-goat anti-rabbit (1:2000)	Jackson Immunores., 111-165-144
Alexa633-goat anti-rabbit (1:2000)	Life Biotech. (Mol. Probes), A21071
Alexa647-donkey anti-rabbit (1:2000)	Life Biotech. (Mol. Probes), A31573
Alexa405-goat anti-mouse (1:2000)	Life Biotech. (Mol. Probes), A31553
Alexa488-donkey anti-mouse (1:2000)	Life Biotech. (Mol. Probes), A21202
Alexa555-goat anti-mouse (1:2000)	Life Biotech. (Mol. Probes), A21424
Alexa647-donkey anti-mouse (1:1000)	Invitrogen, A31571
Alexa555-goat anti-guinea pig (1:2000)	Life Biotech. (Mol. Probes), A21435
Alexa647-goat anti-guinea pig (1:2000)	Life Biotech. (Mol. Probes), A21450
Cy5-donkey anti-guinea-pig (1:400)	Jackson Immunores., 706-175-148
Cy3-donkey anti-rat Fab' (1:400)	Jackson Immunores., 712-166-153
Alexa633-goat anti-rat (1:1000)	Life Biotech. (Mol. Probes), A21094

Bhalerao, S., Berdnik, D., Torok, T. and Knoblich, J. A. (2005). Localization-dependent and -independent roles of numb contribute to cell-fate specification in Drosophila. *Curr Biol* **15**, 1583-1590.

Brand, M., Jarman, A. P., Jan, L. Y. and Jan, Y. N. (1993). *asense* is a *Drosophila* neural precursor gene and is capable of initiating sense organ formation. *Development* **119**, 1-17.

Giagtzoglou, N., Alifragis, P., Koumbanakis, K. A. and Delidakis, C. (2003). Two modes of recruitment of E(spl) repressors onto target genes. *Development* **130**, 259-270.

Kim, J., Sebring, A., Esch, J. J., Kraus, M. E., Vorwerk, K., Magee, J. and Carroll, S. B. (1996). Integration of positional signals and regulation of wing formation and identity by *Drosophila vestigial* gene. *Nature* **382**, 133-138.

Kudron, M. M., Victorsen, A., Gevirtzman, L., Hillier, L. W., Fisher, W. W., Vafeados, D., Kirkey, M., Hammonds, A. S., Gersch, J., Ammouri, H., et al. (2018). The ModERN Resource: Genome-Wide Binding Profiles for Hundreds of Drosophila and Caenorhabditis elegans Transcription Factors. *Genetics* **208**, 937-949.

Skeath, J. B., Wilson, B. A., Romero, S. E., Snee, M. J., Zhu, Y. and Lacin, H. (2017). The extracellular metalloprotease AdamTS-A anchors neural lineages in place within and preserves the architecture of the central nervous system. *Development* **144**, 3102-3113.

Zhu, L. J., Christensen, R. G., Kazemian, M., Hull, C. J., Enuameh, M. S., Basciotta, M. D., Brasefield, J. A., Zhu, C., Asriyan, Y., Lapointe, D. S., et al. (2011). FlyFactorSurvey: a database of Drosophila transcription factor binding specificities determined using the bacterial one-hybrid system. *Nucleic Acids Res* **39**, D111-117.

Supplementary Figure 1

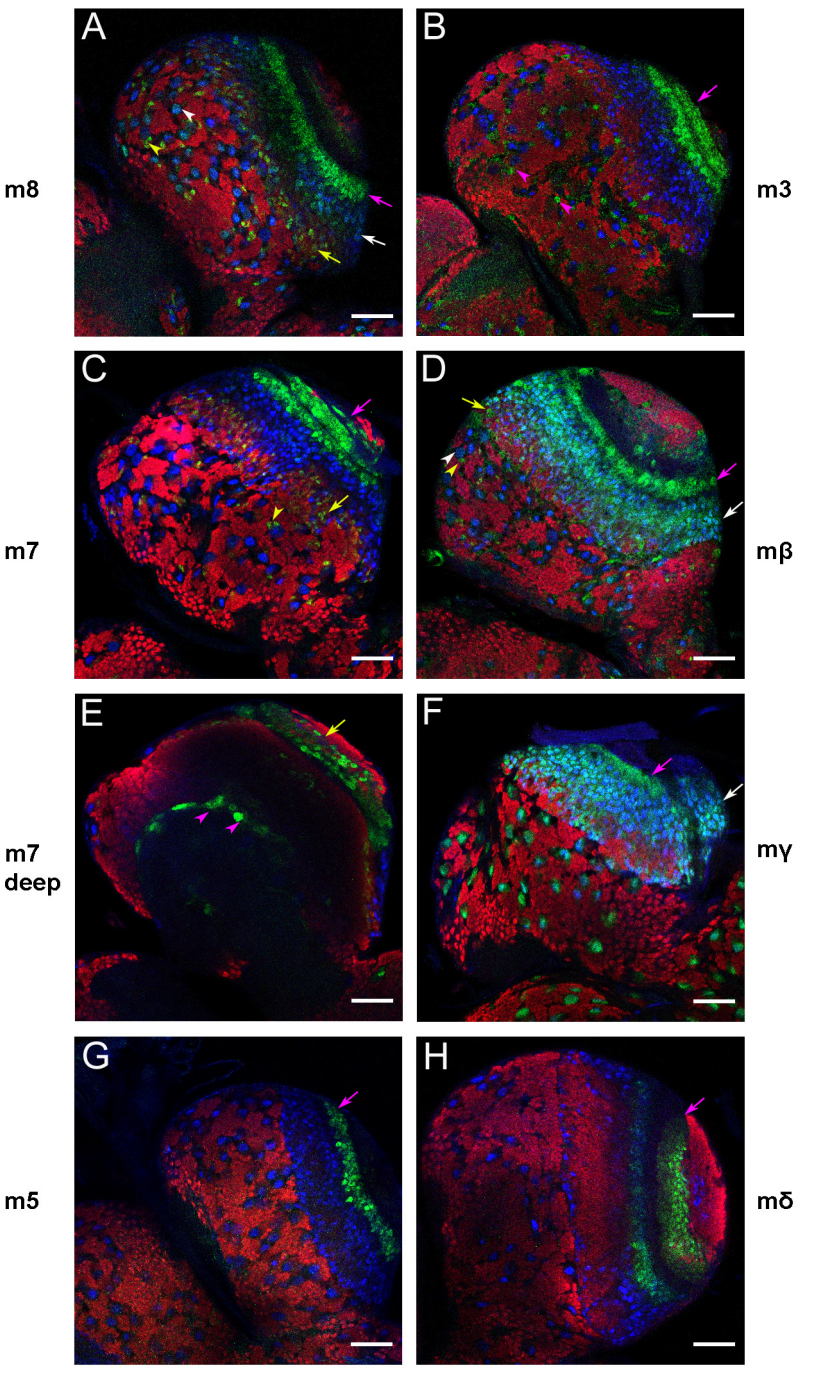

Figure S1 *E(spl)* gene expression in the brain lobe. Each of the seven bHLH E(spl) proteins (m8, m7, m5, m3, mβ, mγ, mδ) was visualized as a GFP fusion from a transgenic genomic BAC transgene (Kudron et al., 2018). E(spl)-GFP is green, Dpn (NSCs) blue and Elav (neurons) red in all panels. In the central brain, white arrowheads mark NSCs; yellow arrowheads mark GMCs/early neurons; magenta arrowheads mark glia. In the optic lobe, white arrows mark medulla NSCs, yellow arrows mark GMCs/early neurons and magenta arrows mark other structures, like the very prominent neuroepithelium. All panels show ventral superficial sections, except E, which shows a deep cortical section to highlight neuropil glia expression of E(spl)m7. Scalebars 50µm.

Supplementary Figure 2

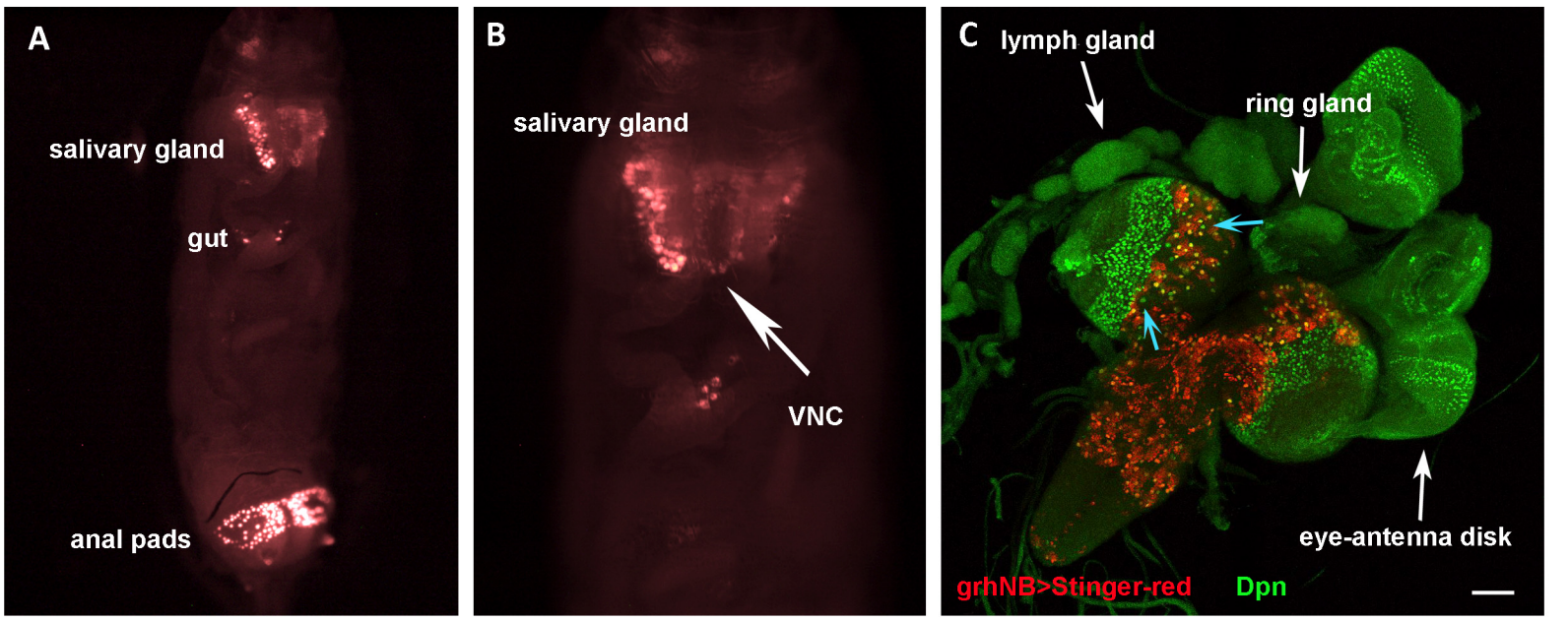

Figure S2 Expression pattern of the grhNB-Gal4 driver. A-C Revealed by UAS-Stinger-red; D,E revealed by UAS-CD8-GFP. A,B: third instar larva viewed under the stereoscope shows prominent expression in salivary glands and anal pads and weaker expression in the CNS (VNC is discernible in the higher magnification, B); a few sporadic positive intestinal cells are also visible. C: 100µm thick projection of a CNS and attached tissues, as marked. Note that grhNB-Gal4 expresses only in central brain and VNC lineages, as well as a few VNC midline cells. No other CNS structure and no other tissue seen in this view (imaginal disks, ring gland or lymph gland) expresses grhNB. D, E: single confocal sections of brain lobes to highlight that grhNB expresses in the majority of, but not all, NSC lineages. Examples of non-expressing NSCs/INPs are marked with blue arrows in C-E. Scalebars in C-E 50µm.

Supplementary Figure 3

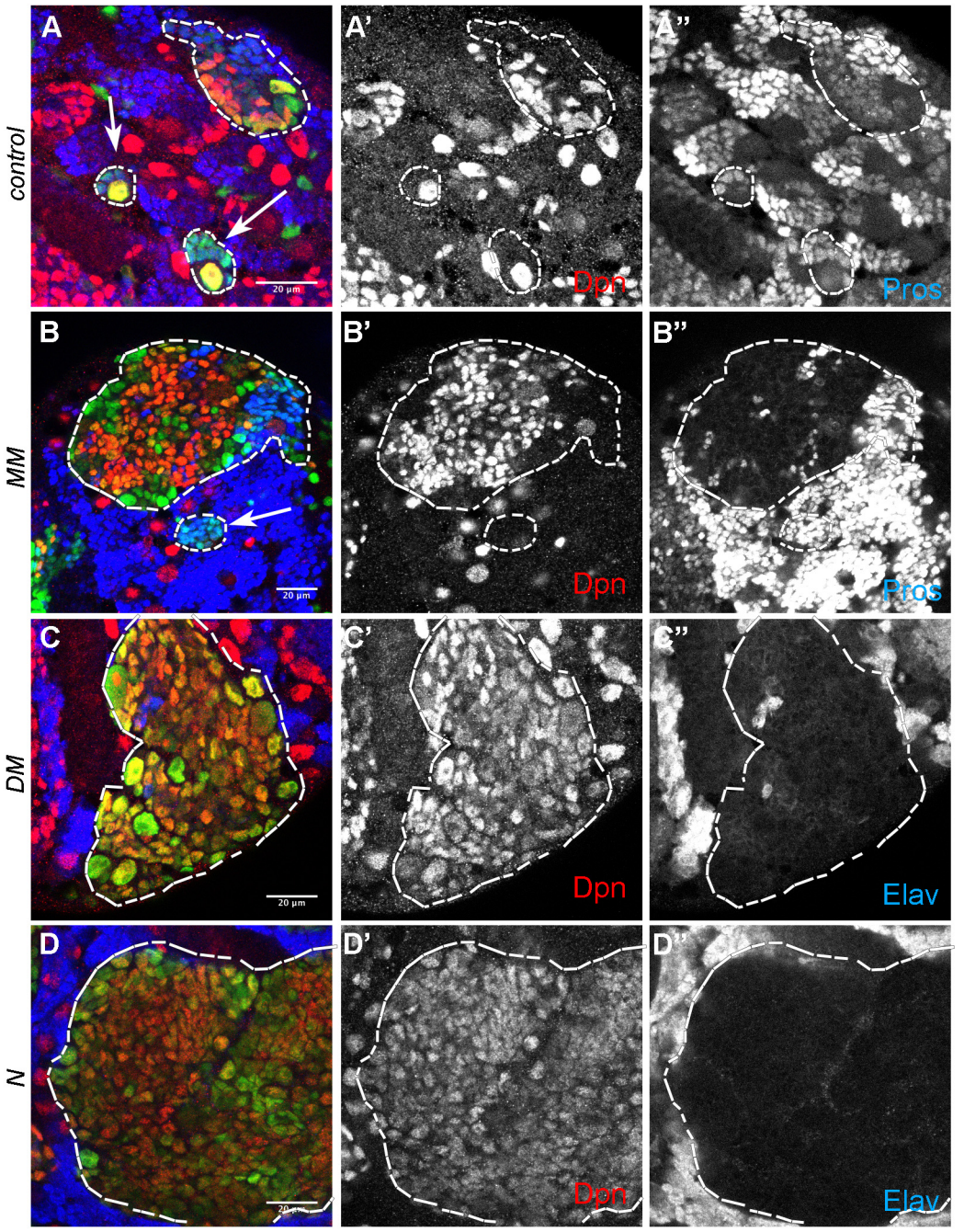

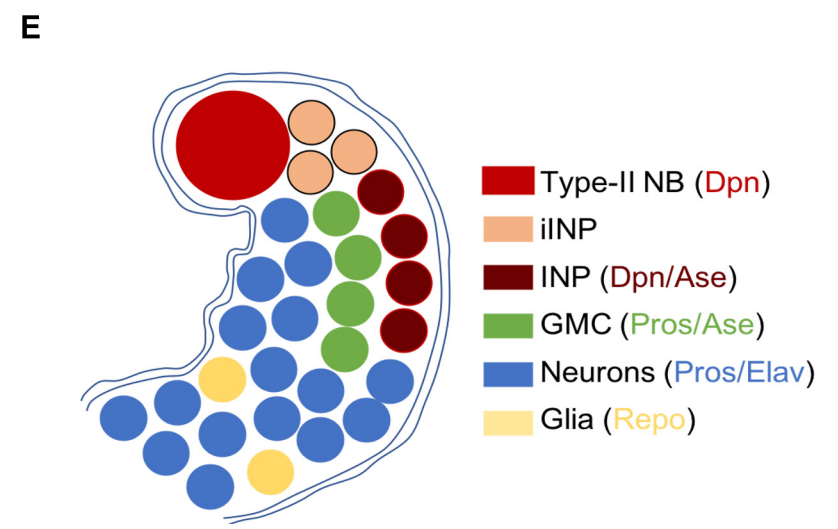

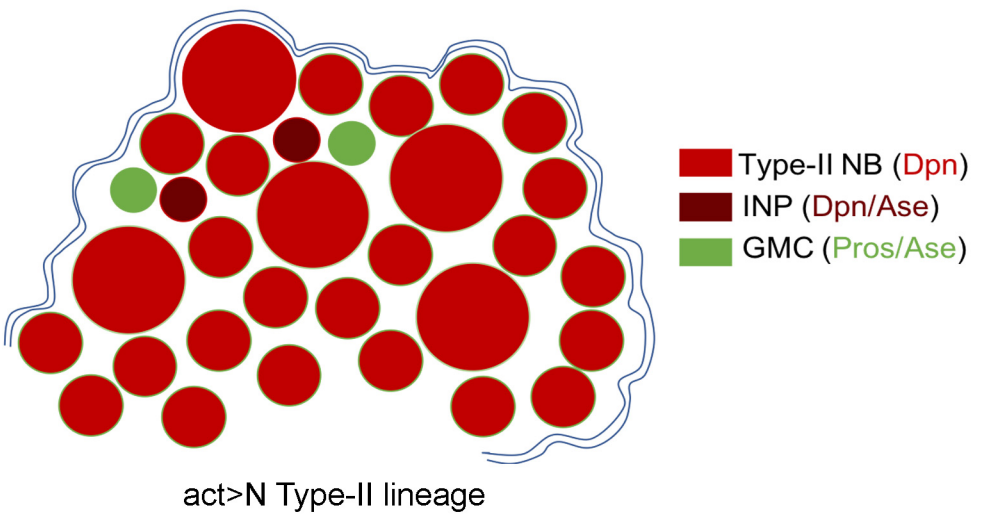

Figure S3 Notch and Hes induced hyperplasia in Type II lineages. Panels A-D are stained to reveal NSCs (Dpn, red) and (A,B) GMCs/neurons (Pros, blue) or (C,D) neurons (Elav, blue). FLP-out clones are marked with GFP (green) and overexpress (A) GFP alone (control); (B) UAS-m8, UAS-mγ (MM); (C) UAS-dpn, UAS-mγ (*DM*); (D) UAS-NΔecd (N). Clones are outlined. In panels A and B adjacent smaller Type I clones are also outlined and marked with an arrow. (E) Cartoons depict the cellular composition of wt vs *N* overexpressing TypeII lineages. *MM* and *DM* lineages would be the same, only they should additionally have a few blue cells (neurons). Scalebars 20µm.

Supplementary Figure 4

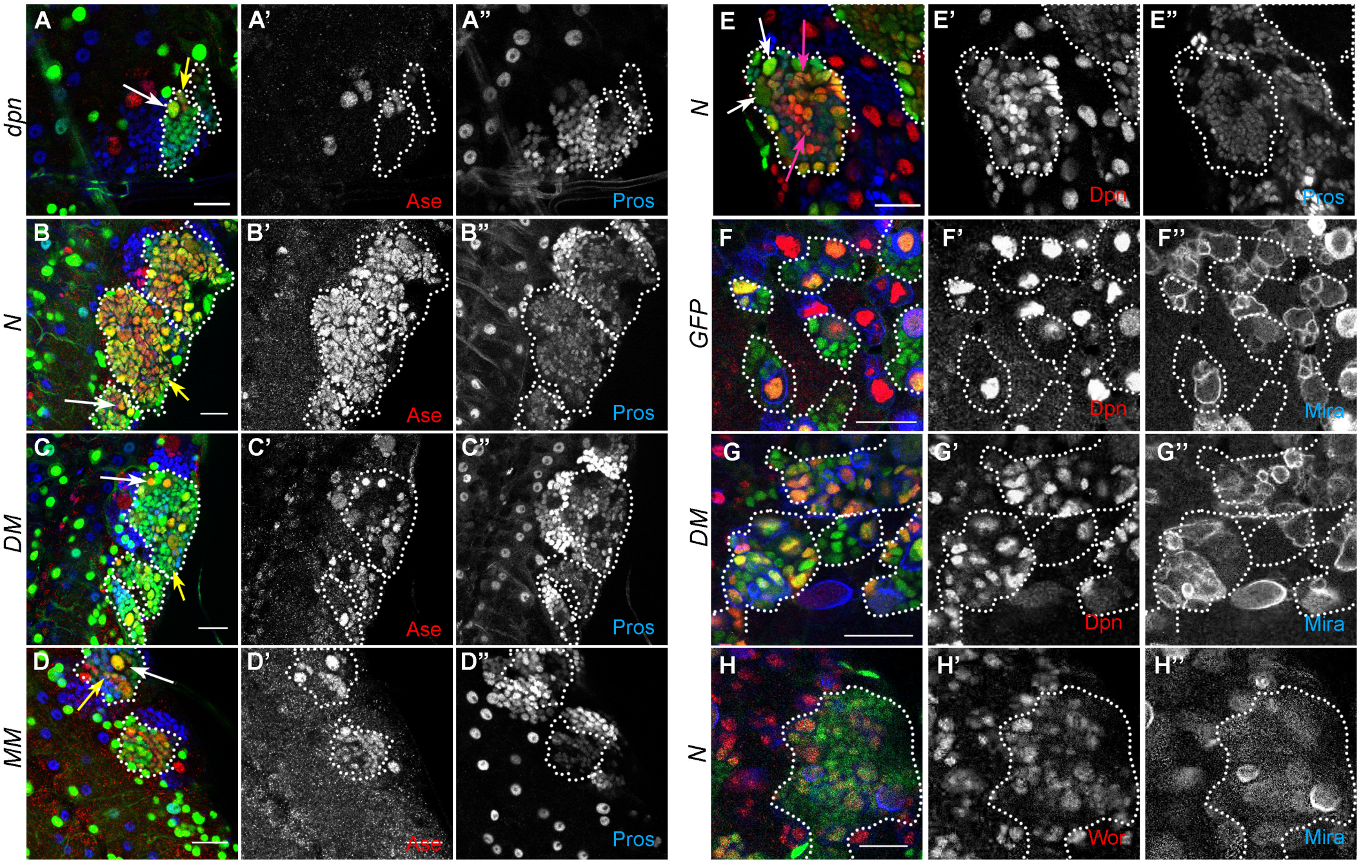

Figure S4 Further examples of NSC hyperplasia caused by N/Hes overactivity. All panels show *act>STOP>Gal4* clones expressing GFP and transgenes as marked. A-D: NSCs/GMCs are detected by Ase (red); GMCs/young neurons are detected by Pros (blue). A is essentially wt, as *dpn* expression alone rarely causes any defects in Type I lineages. White arrows mark examples of Ase positive/ Pros negative (NSC-like) cells. Yellow arrows mark double-positive (GMC-like) cells. E: Examples of aberrant Dpn/Pros double positive cells indicated by magenta arrows; white arrows point to Dpn positive/ Pros negative NSC-like cells. (F-H) NSCs are marked by Dpn or Wor (red); NSCs/GMCs marked by Mira (blue). A-D are taken from VNCs; E-H are from brain lobes. Scalebars 20µm.

Supplementary Figure 5

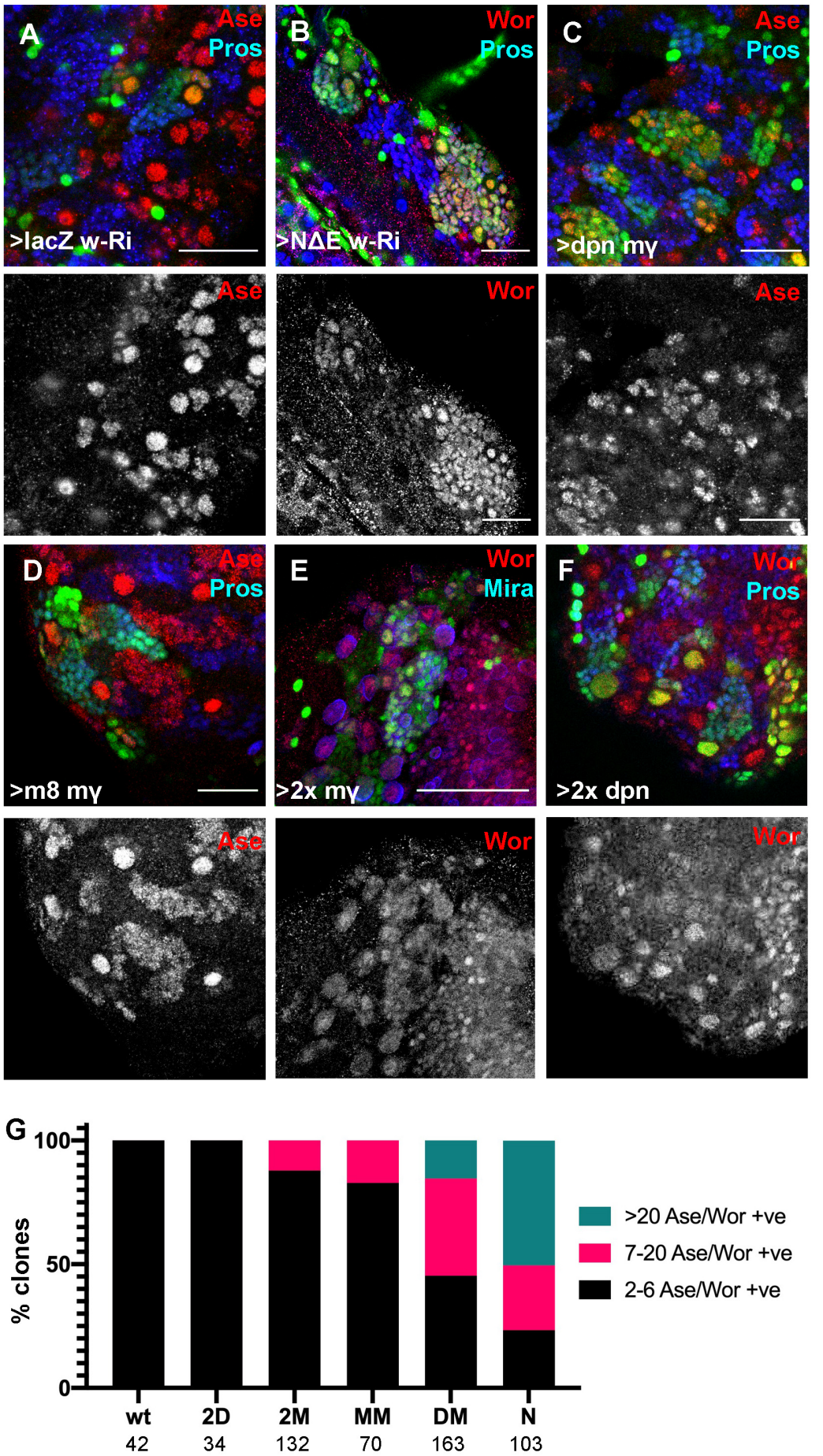

Figure S5 Comparison of phenotypic severity in act>STOP>Gal4 clones. All panels show 3d old clones from misexpression of two transgenes. w-Ri is a UAS-white RNAi neutral transgene for dosage equalization. lacZ is also a neutral UAS-lacZ transgene. The UAS transgenes misexpressed are shown at the bottom of each panel. A,D,E,F are clones from brain lobes; B & C are clones from VNCs. A NSC/GMC marker (red) is used in each panel, either Wor or Ase, as indicated. A-D & F are counterstained with Pros (blue), whereas in E we used another NSC marker, Mira (blue). G shows the distribution of wt-looking (black) or NSC-hyperplastic (red/ green) Type I clones. NSCs were detected using either Ase or Wor, both of which also mark GMCs. The total number of clones scored is shown at the bottom.

Supplementary Figure 6

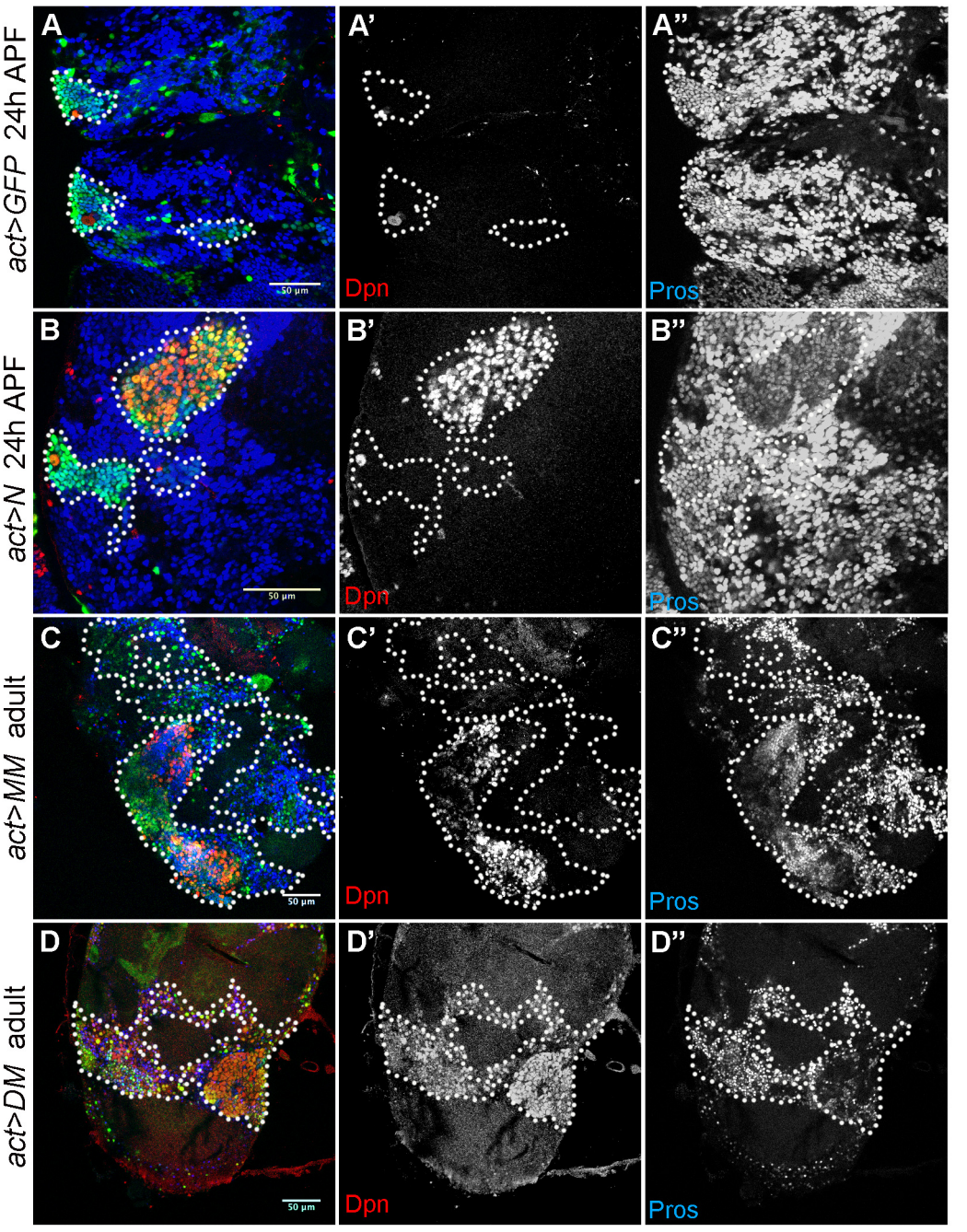

Figure S6 N/Hes NSC hyperplasias persist after pupariation. A,B: brain lobes dissected at 24h APF; C,D: brain lobes dissected from freshly eclosed adult escapers. All animals expressed GFP together with the indicated transgenes from an act>STOP>Gal4 driver after hsFLP induction at early larval stages. Dpn is stained red and Pros blue. Individual channels shown in greyscale. The two clones that retain a Dpn-positive NSC in the wt (A) are mushroom body lineages that continue proliferating into the early pupal stages. Note that in the early pupa Pros, an immature neuron marker, is still widely expressed in normal tissue (but repressed in one N clone), whereas it is turned off in the adult. However MM and DM clones exhibit persistence of Pros into adulthood. Scalebars 50µm.

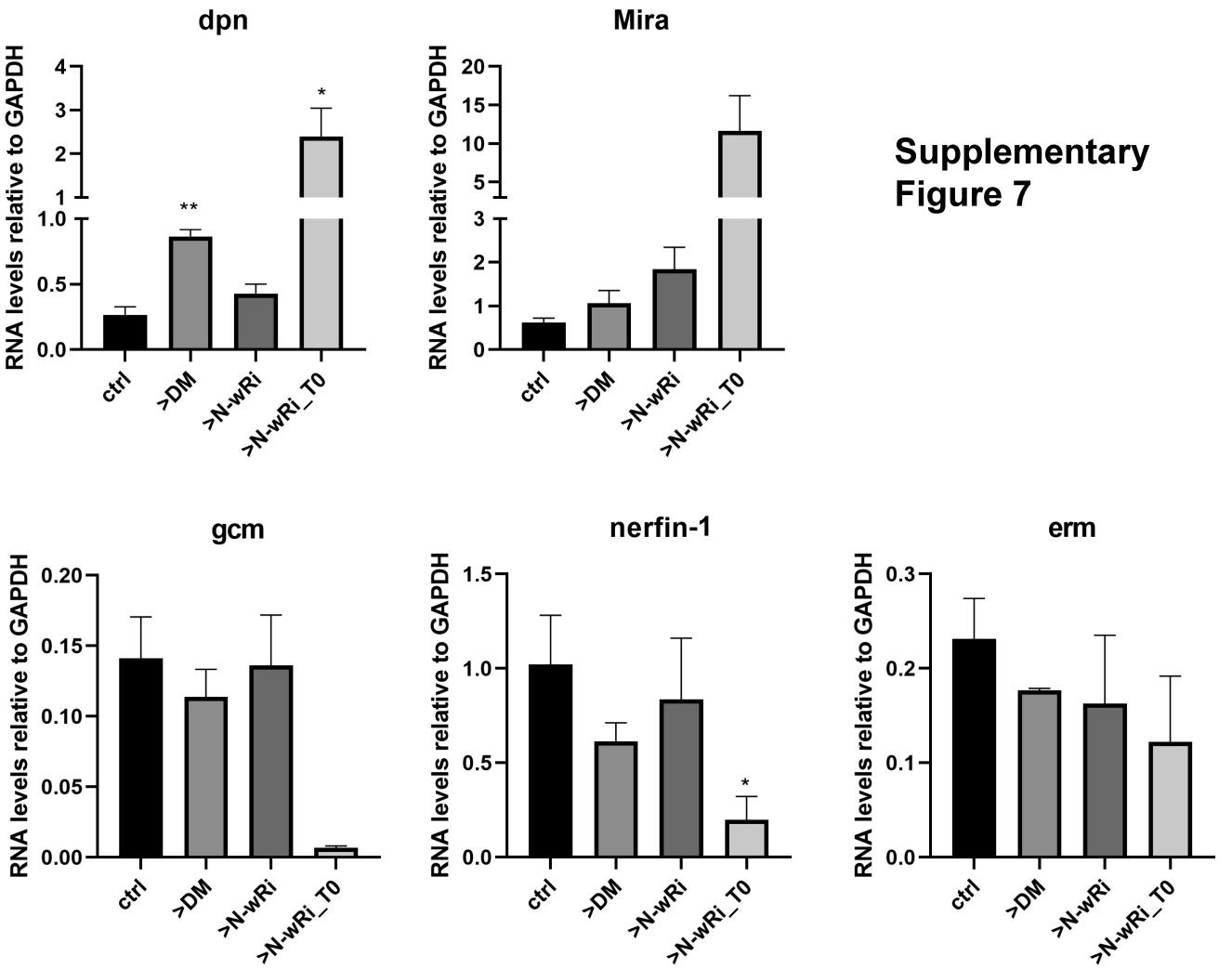

Supplementary Figure 7

Figure S7 qPCR validation of select mRNAs. Expression levels were calculated by q-RT-PCR from *DM* or *N+wRNAi* overexpressing CNSs (using *tub-Galt80^{ts} grhNB-Gal4*) or wt (*lacZ+wRNAi*) controls. Animals were raised at 18°C for 8 days and shifted to 30°C 48 hours prior to dissection and RNA collection. An allografted tumour sample was also included (>N-wRi_T0), which came from tumour recovered 8-10 days after transplanting *tub-Gal80^{ts}, grhNB>N+wRNAi+RFP* brain lobes into wt hosts. Expression levels are shown relative to *GAPDH* mRNA. Error bars show the standard error of the mean from triplicate measurements (dpn, Mira, erm) or standard deviation from duplicate measurements (gcm, nerfin1). Asterisks indicate samples that are significantly different from control by Student's t-test (* P<0.05, **P<0.01). Although the values show a large degree of variability, stem cell genes (*dpn, Mira*) show an upward trend, whereas differentiation genes (*gcm, nerfin-1, erm*) show a downward trend. Both trends continue after transplantation (T0).

Supplementary Figure 8

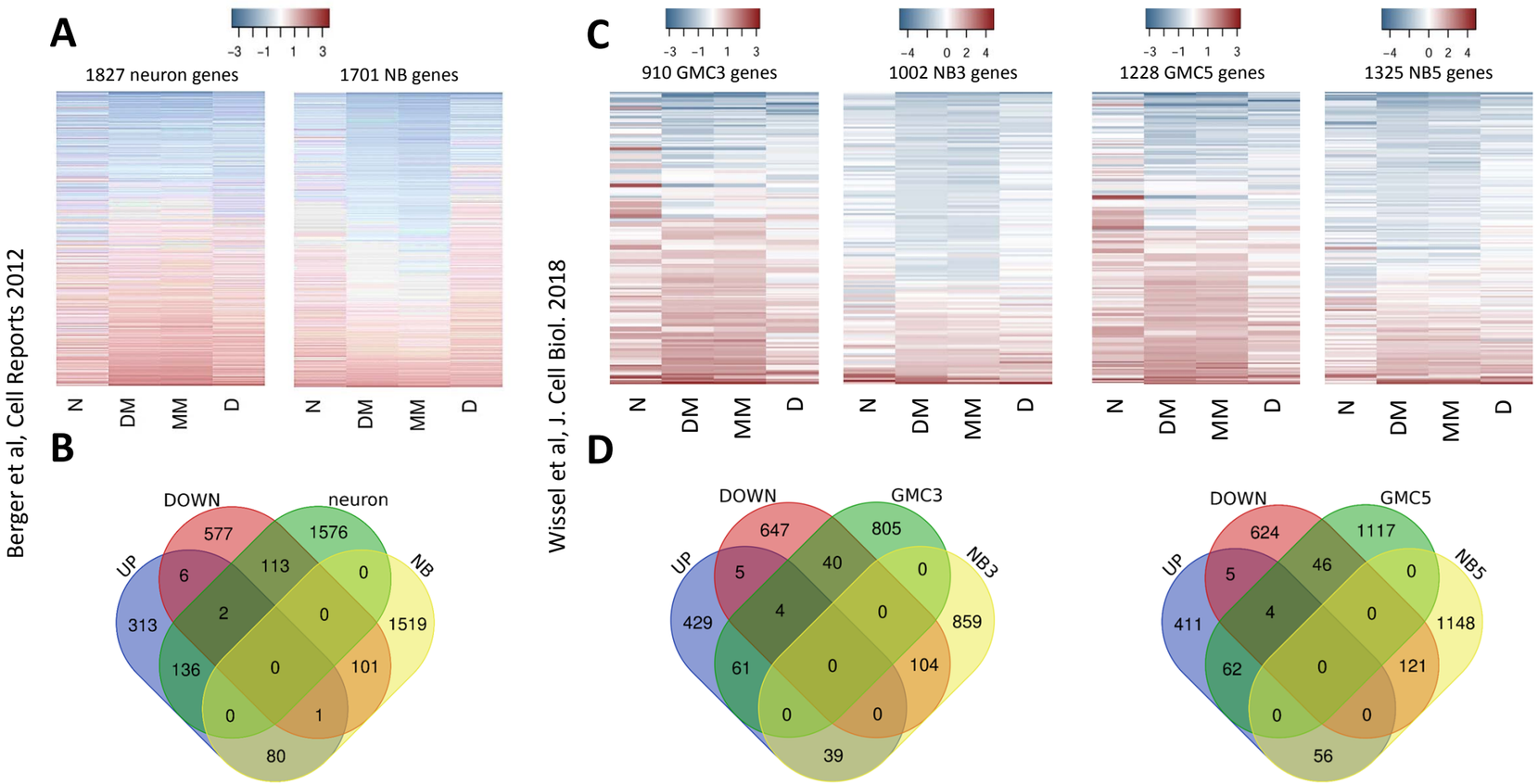

Figure S8 Comparison of N/Hes differentially regulated genes with neuron, GMC and NSC-enriched gene-sets. (A,B) Comparison with the neuron vs NSC enriched genes defined by Berger et al (2012): genes that show differential expression in FACS-sorted neuron or NSC populations from wt CNSs. (A) Heatmaps showing the $\log_2$(fold-change) of neuron-enriched genes (left) and NSC-enriched genes (right) in the N and Hes overexpression backgrounds. (B) Venn diagram showing overlap of high confidence (FDR≤ 0.05) UP or DOWN-regulated genes in the N/Hes conditions (union of *N* with *DM* and *MM*, ie the 573 genes of Figure 3B and the 829 genes of Figure 3C; some duplicates removed) with the neuron vs NSC enriched gene-sets. (C, D) Comparison with the NSC vs GMC enriched genes defined by Wissel et al (2018): dissociated NSCs were cultured in vitro and their smaller GMC progeny FACS-sorted from the larger NSCs. 3 and 5 refer to the hours of culturing. (C) Heatmaps showing the $\log_2$(fold-change) of GMC-enriched genes and NSC-enriched genes from each culture timepoint in the N and Hes overexpression backgrounds. (D) Venn diagram showing overlap of high confidence (FDR≤ 0.05) UP or DOWN-regulated genes in the N/Hes conditions (as in B) with the GMC vs NSC enriched gene-sets from the two culture timepoints.

Supplementary Figure 9

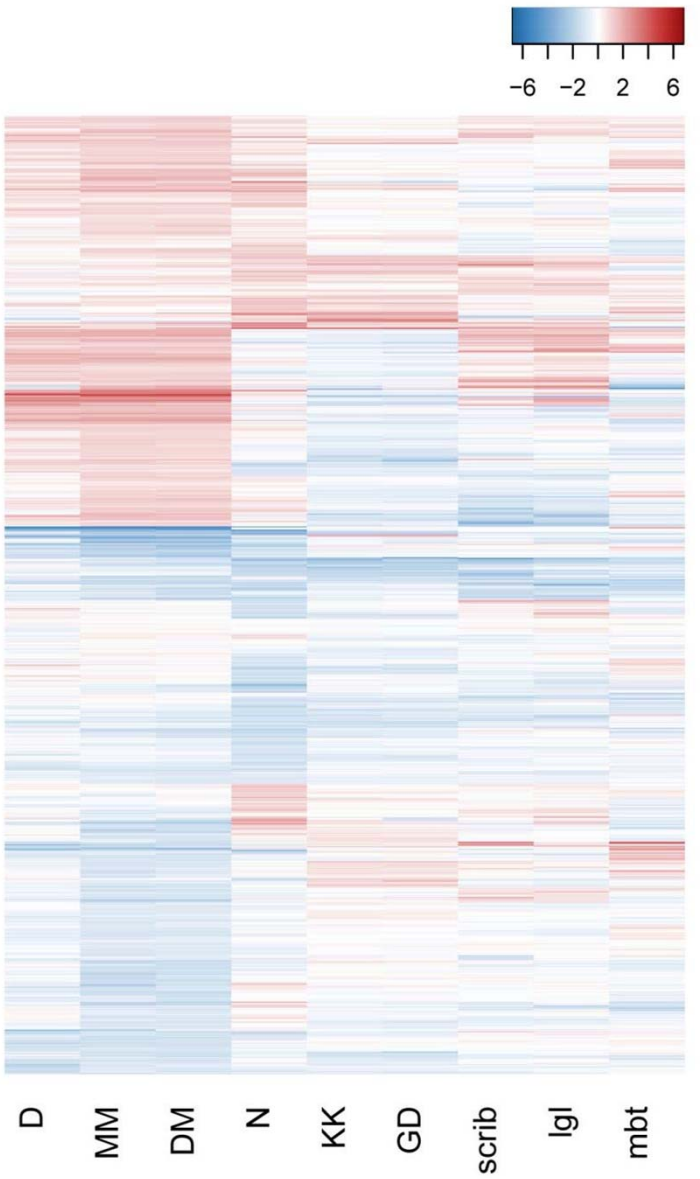

Figure S9 Comparison of N and Hes CNS tumours with other CNS tumours. Heat map of the fold-change of the 1410 genes selected by differential expression in the N or Hes tumours (Figure 3A) in five additional tumour transcriptomes. KK and GD are two *brat* RNAi genotypes, whereas scrib, lgl and mbt refer to homozygous mutant larval CNSs for the genes *scrib*, *l(2)gl* and *l(3)mbt*, respectively, all of which show CNS hyperplasia.

Supplementary Figure 10

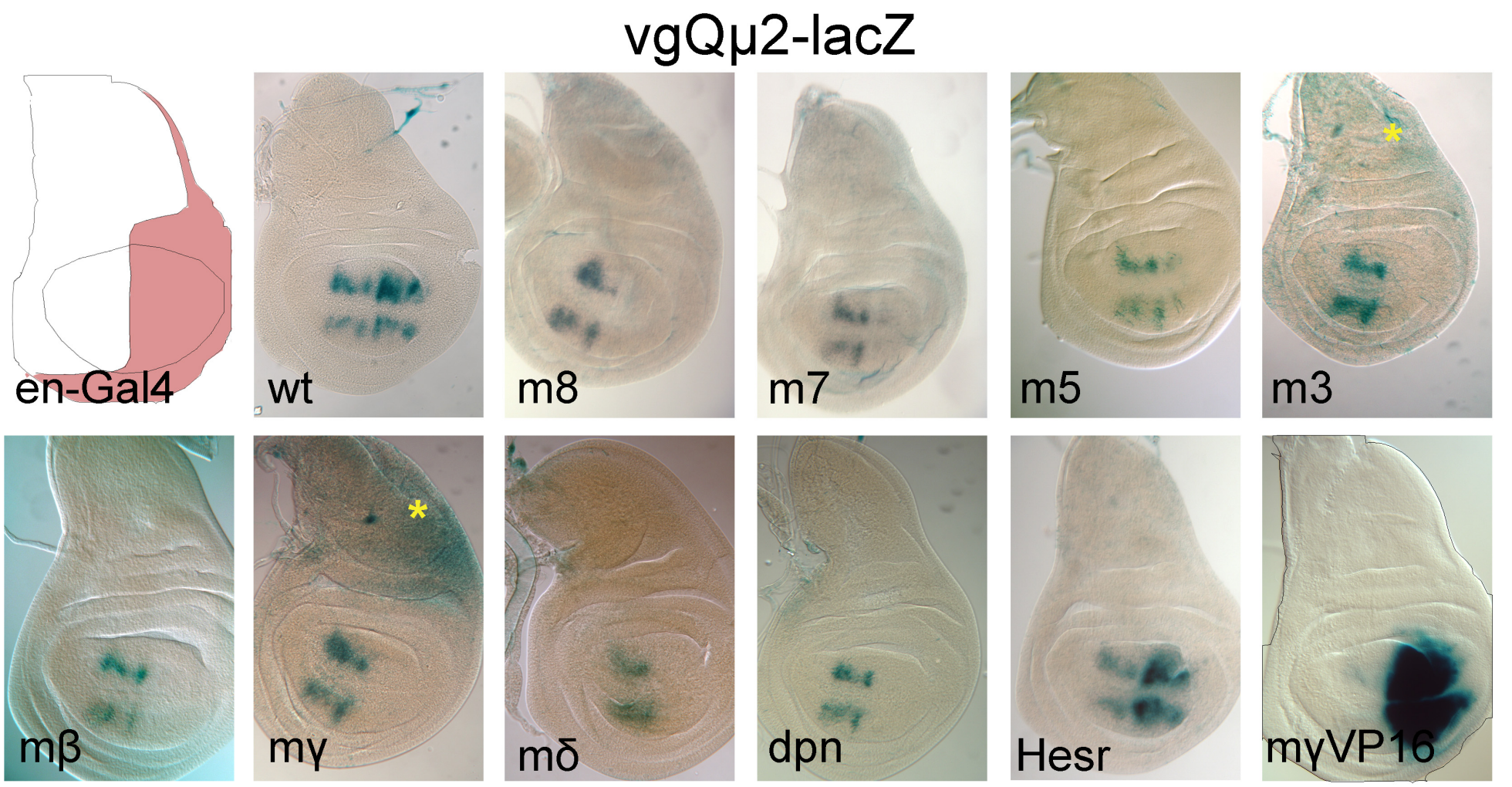

Figure S10 Transcriptional activity of fly Hes proteins assayed by the *vgQμ2-lacZ* reporter. All panels show third instar larval wing disks carrying the *vgQμ2-lacZ* reporter and the *en-Gal4* driver, whose expression pattern is shown in the first panel in pink. The UAS responders used in each case are shown; wt: no UAS responder used. All disks were incubated in Xgal for 24-48h, except UAS-mγVP16, which was developed for 6h. Some disks show background staining due to the prolonged Xgal incubation time (yellow asterisks). It is clear that all E(spl) proteins (m8, m7, m5, m3, mβ, mγ, mδ) and Dpn repress the reporter. The artificial activator mγVP16(Giagtzoglou et al., 2003) activates strongly, whereas Hesr activates weakly. The *vgQμ2* reporter is based on the 820bp *vg*-quadrant enhancer(Kim et al., 1996), which bears a single Hes consensus target site (aggCACGCGgca, capitals indicate the E_C-box core). In the *μ2* mutant(Koumpanakis, 2007) we have mutated two nucleotides in that site (to *t*ggCACGCG*c*ca) to improve Hes protein binding(Jennings et al., 1999; Zhu et al., 2011).

Supplementary Figure 11

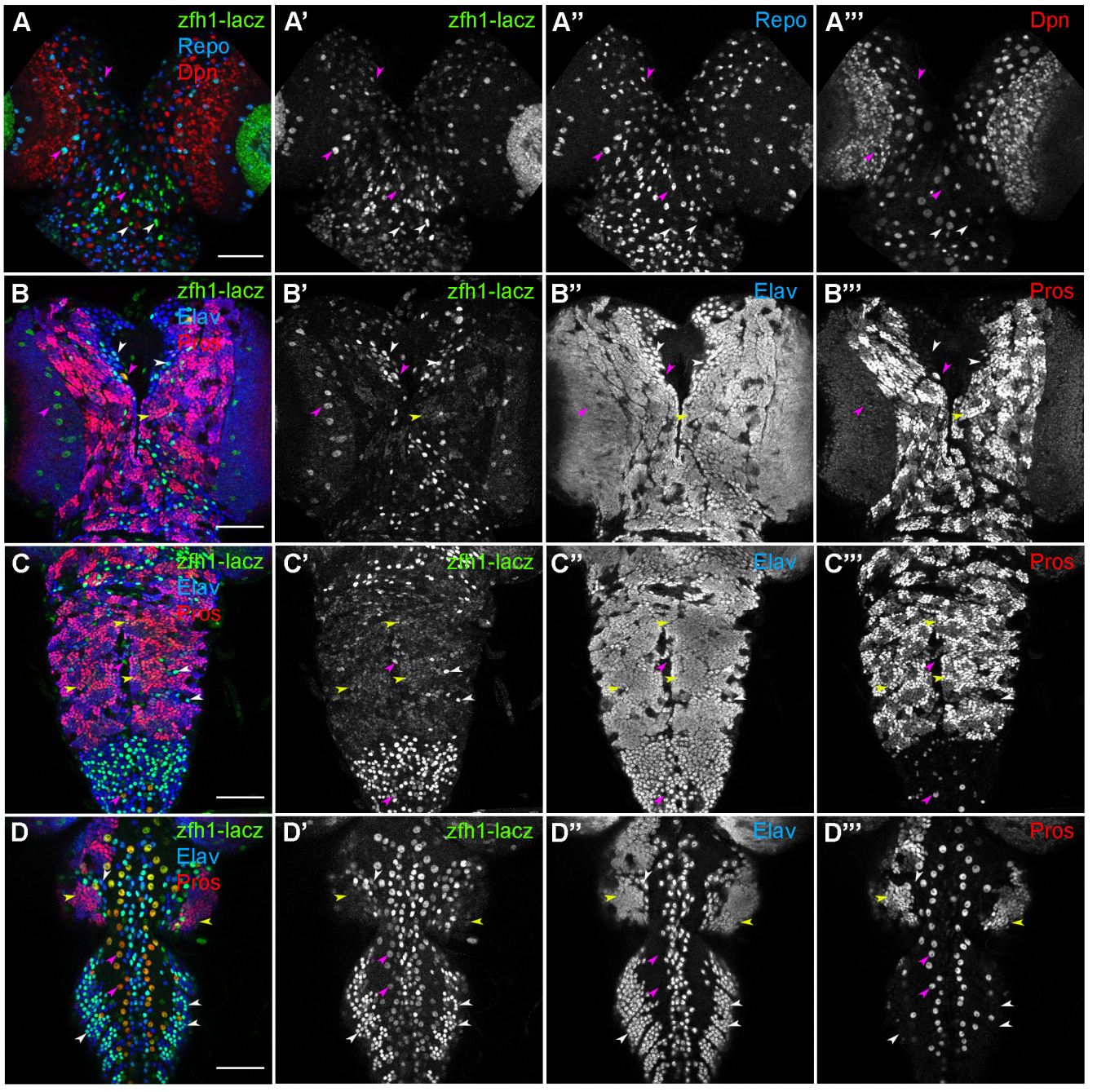

Figure S11 *zfh1-lacZ* expression in the wt. β-galactosidase from *zfh1-lacZ*^{00865} is green in all panels. 4µm-thick projections near the CNS surface. (A) Brain lobes counterstained with glial marker Repo (blue) and NSC marker Dpn (red). (B-D) Counterstaining for neuronal marker Elav (blue) and GMC/young neuron marker Pros (red) – note that Pros is also expressed in some glial cells. (B) Brain lobes. (C-D) VNC, ventral side (C) and dorsal side (D). Examples of zfh1-positive GMCs/early neurons (Pros and Elav positive) are shown with yellow arrowheads, mature neurons (Elav positive/ Pros negative) by white arrowheads and glia (Repo or Pros positive/ Elav negative) by magenta arrowheads. Scalebars 50µm.

Supplementary Figure 12

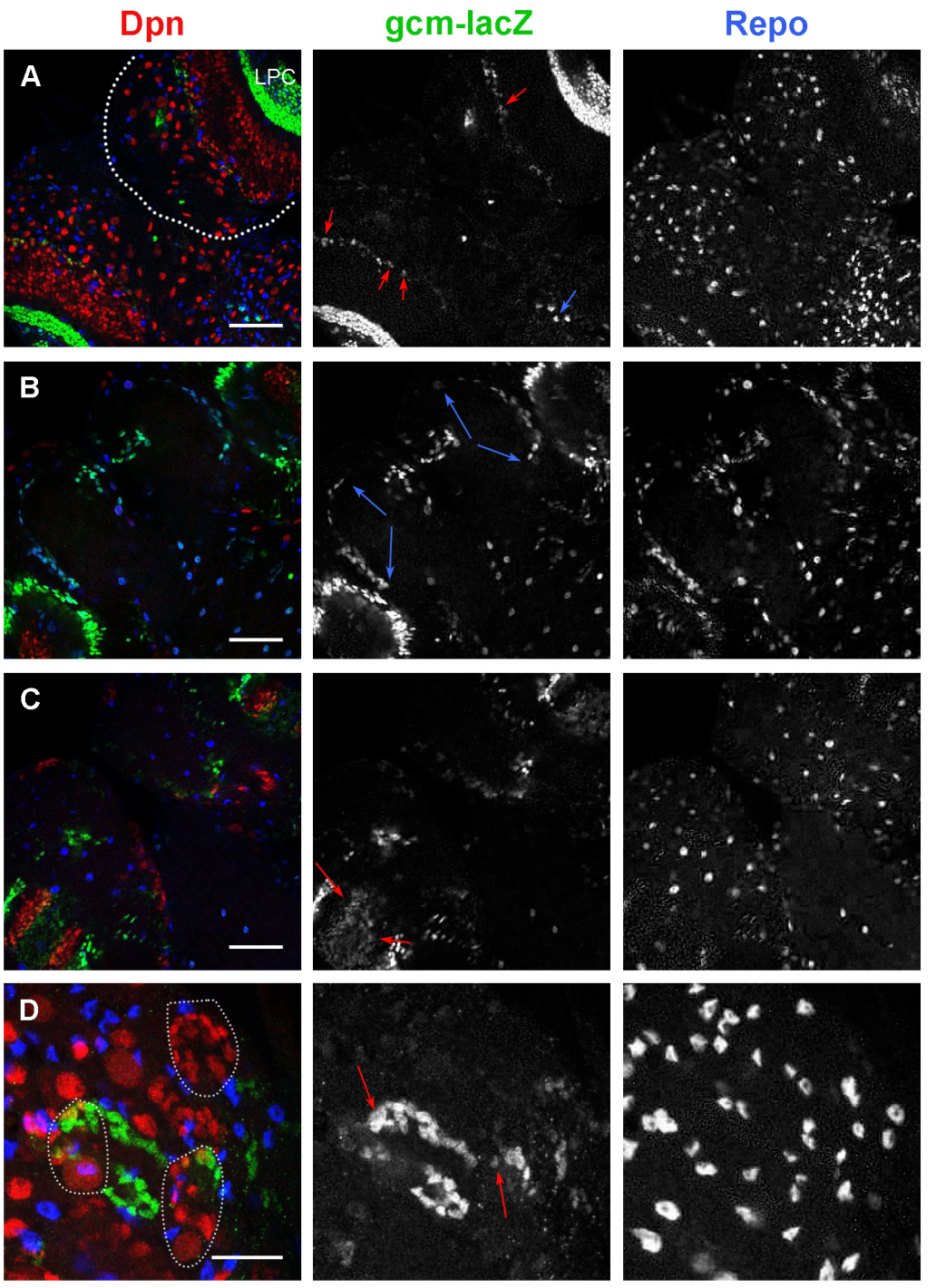

Figure S12. gcm expression in the third instar CNS. A-C are single confocal sections from the same CNS (the right brain lobe is outlined in A/ anterior is top left) at different focal planes. In the gcm-lacZ channel, red arrows mark selected nuclei that are also Dpn positive, whereas blue arrows mark selected nuclei that are Repo positive. At the surface (A) gcm is expressed in lamina precursors (LPC) and few scattered cells, some of which (red arrows) are at the medial edge of the medulla NSCs (Dpn-positive). Most glia in this section (mostly cortex glia, marked by Repo, blue) are gcm-negative or weakly positive. B is 30µm below A; the majority of gcm-positive cells are also Repo-positive. The blue arrows mark the arcs of neuropil glia. C is 22 µm deeper than B; some overlap is seen between gcm expression and inner proliferation centre NSCs (red arrows). D is a maximum projection (5µm thick) of an area containing Type II lineages, the estimated extent of some of which is shown by dotted outlines. Overlap of gcm-lacZ with small Dpn-positive nuclei (INPs) is shown with red arrows. Scalebars A-C = 50µm/ D= 20µm.

Supplementary Figure 13

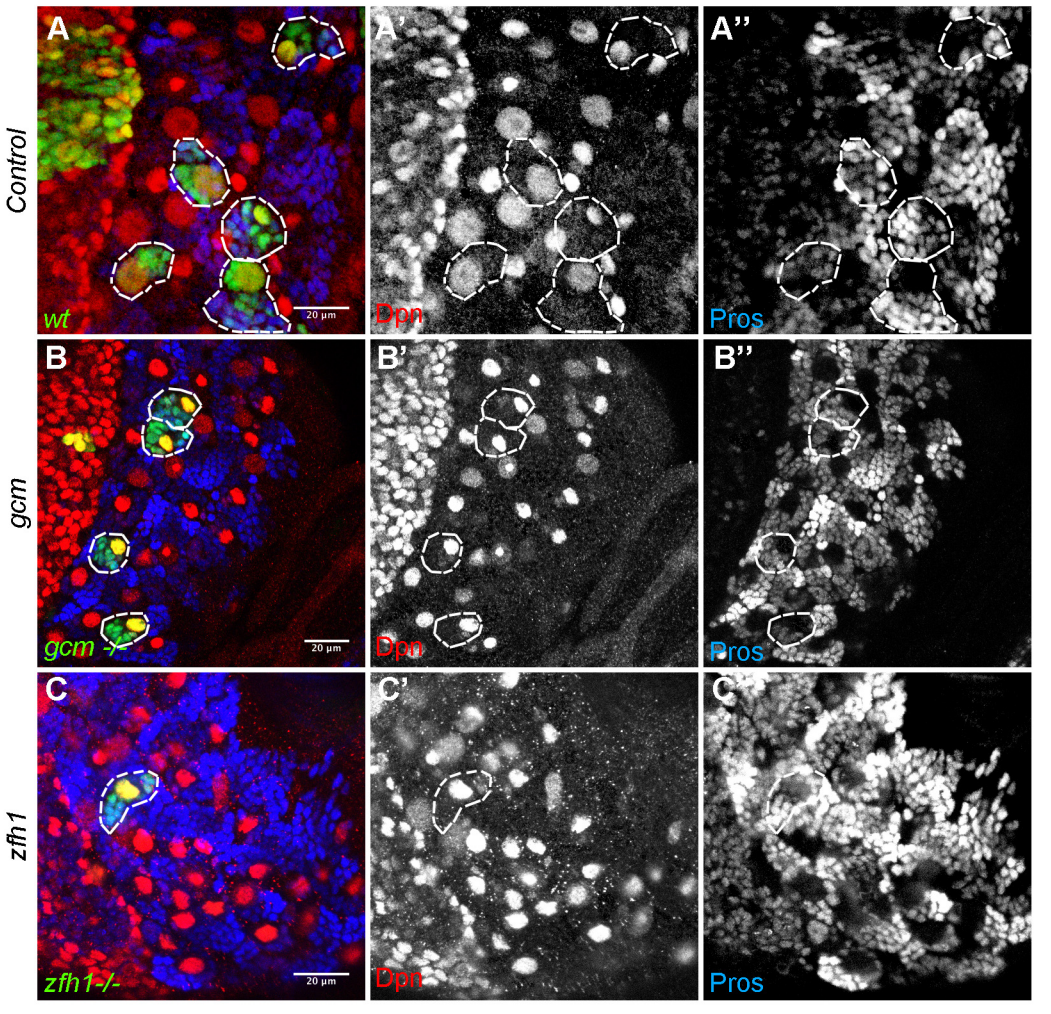

Figure S13 Loss-of-function analysis of *zfh1* and *gcm*. MARCM clones are marked with GFP (green) and traced by dashed outlines. (a) WT, (B) clones homozygous for gcm^{N7-4} (C) clones homozygous for $zfh1^{75.26}$. NSCs are imaged by Dpn (red) and GMCs/young neurons by nuclear Pros (blue). Individual channels shown in greyscale. Scalebars 20µm.

Supplementary Figure 14

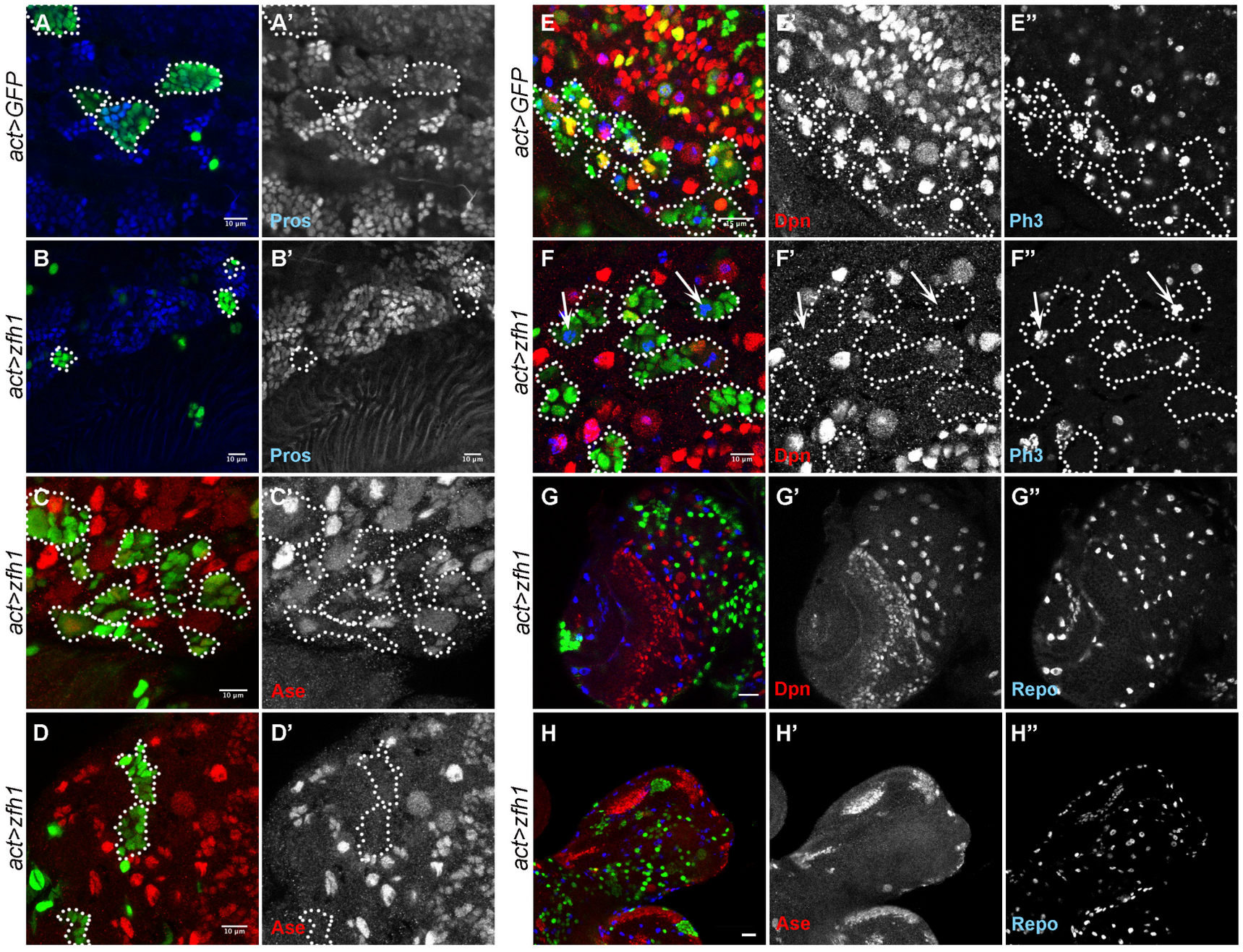

Figure S14 Effect of *zfh1* misexpression on CNS lineages. *act>STOP>Gal4* FLPout clones are marked by GFP (green) and traced with dotted outlines. (A) wt clones 3d ACI stained for Pros (blue, shown separately in A'). (B) *UAS-zfh1* clones 2d ACI stained for Pros (blue, shown separately in B'). (C,D) *UAS-zfh1* clones 1d (C) or 2d (D) ACI stained for Ase (red) shown separately in C', D'. (E) wt clones 1d ACI stained for Dpn (red) and the mitotic marker phospho-H3 (blue). (F) *UAS-zfh1* clones 1d ACI stained as in E. Arrows point to large mitotic cells (NSC-like) that are Dpn negative. (G,H) Examples of brain lobes carrying *UAS-zfh1* clones 3d ACI and stained for the glia marker Repo (blue) and Dpn (red) in G or Ase (red) in H. G is a more superficial section than H. Zfh1-overexpressing cells (green) do not overlap with Repo-positive glia (blue). A-D scalebars 10µm, E scalebar 15µm, F scalebar 10µm, G-H scalebars 15µm.

Supplementary Figure 15

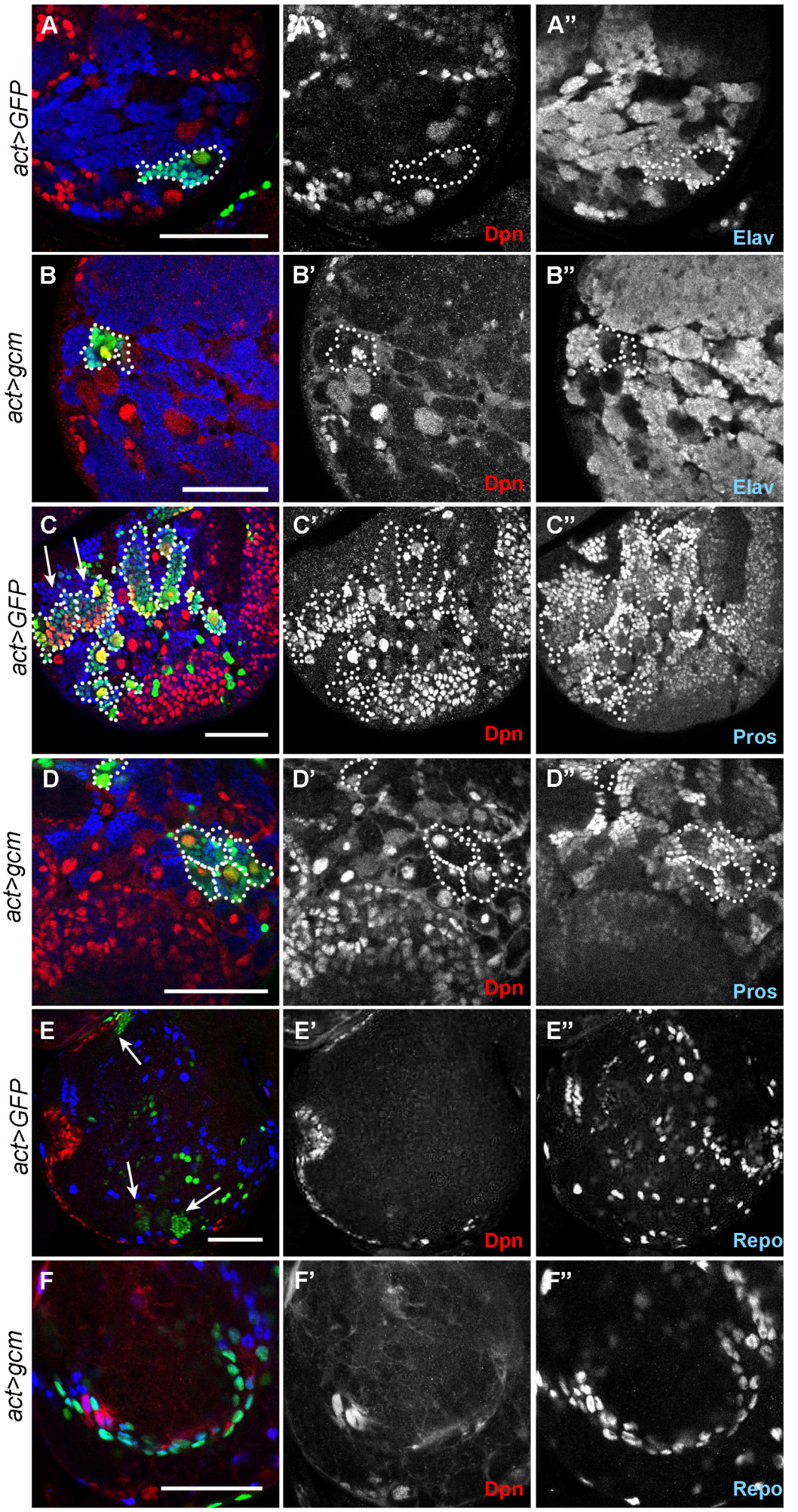

Figure S15 Effect of *gcm* misexpression on CNS lineages. *act>STOP>Gal4* FLPout brain lobe clones are marked by GFP (green) and traced with dotted outlines. (A,C,E) Control clones (GFP only); (B,D,F) UAS-gcm clones. (A,B) Sample stained for Dpn (NSCs, red) and Elav (neurons, blue). (C,D) Sample stained for Dpn (NSCs, red) and Pros (GMCs/ young neurons, blue); note two Type II clones in C (arrows). (E,F) Sample stained for Dpn (NSCs, red) and Repo (glia, blue). In E and F deep sections are shown where clone cells may have migrated away from the superficial stem cell (superficial lineages marked by arrows in E; note that the upper one derives from the OL); in E there is hardly any GFP marking of glia, whereas in F most clonal cells have adopted a glial fate. All scalebars 50µm.

Supplementary Figure 16

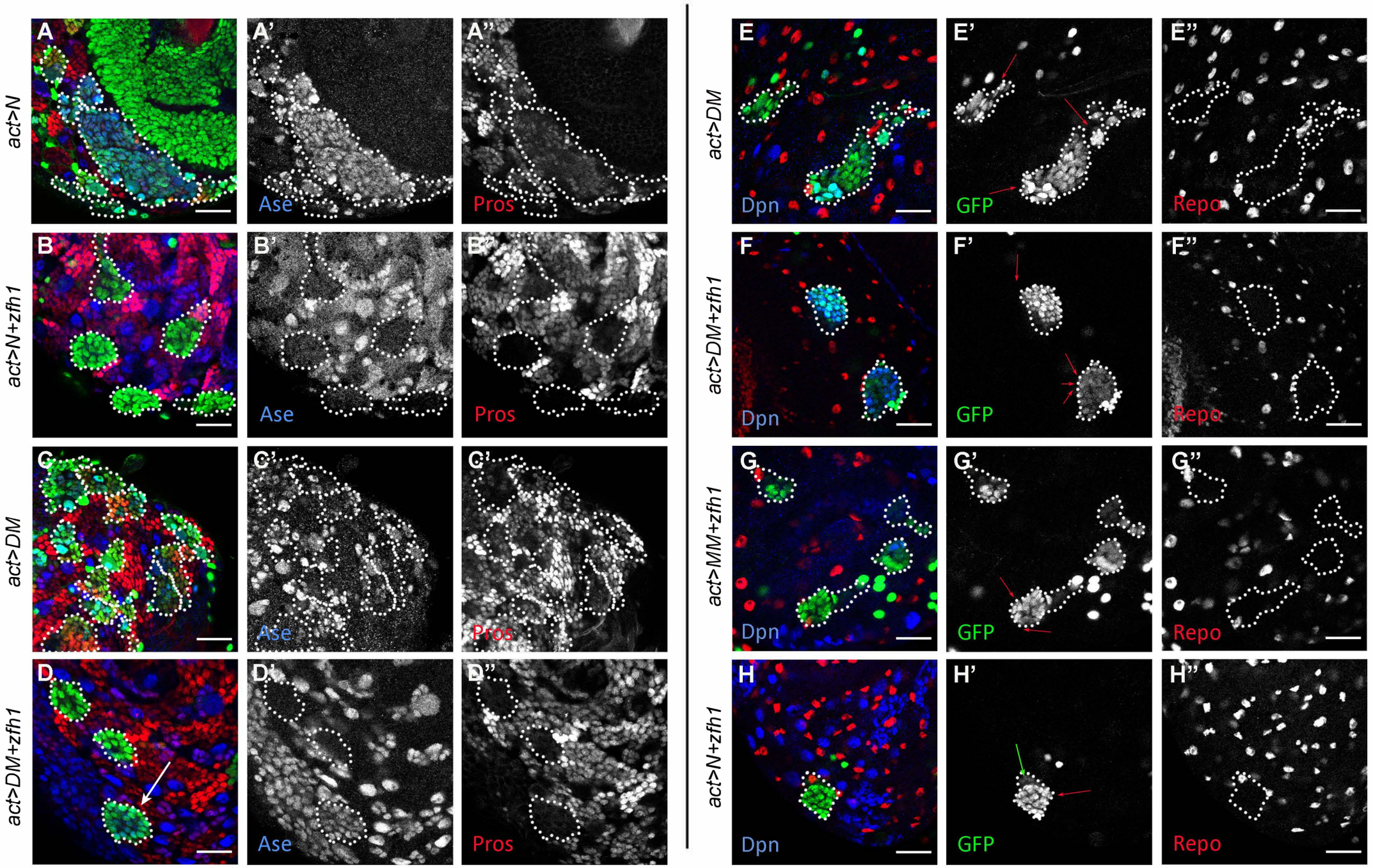

Figure S16 Effect of *zfh1* misexpression on *N*, *DM* and *MM* lineages. *act>STOP>Gal4* FLPout brain lobe clones are marked by GFP (green) and traced with dotted outlines. (A-D) Effects on Ase (blue) and Pros (red). Most Type I N/Hes clones lose Ase and Pros upon zfh1 expression, with some exceptions (arrow in D, no loss of Ase). (E-H) Effects on Repo: Zfh1 does not induce gliogenesis. Even though there are several Repo positive cells adjacent to clones (red arrows), there are very few within clones (green arrow in H'). In E-H blue is Dpn. All panels are from brain lobes. Scalebars 25µm.

Supplementary Figure 17

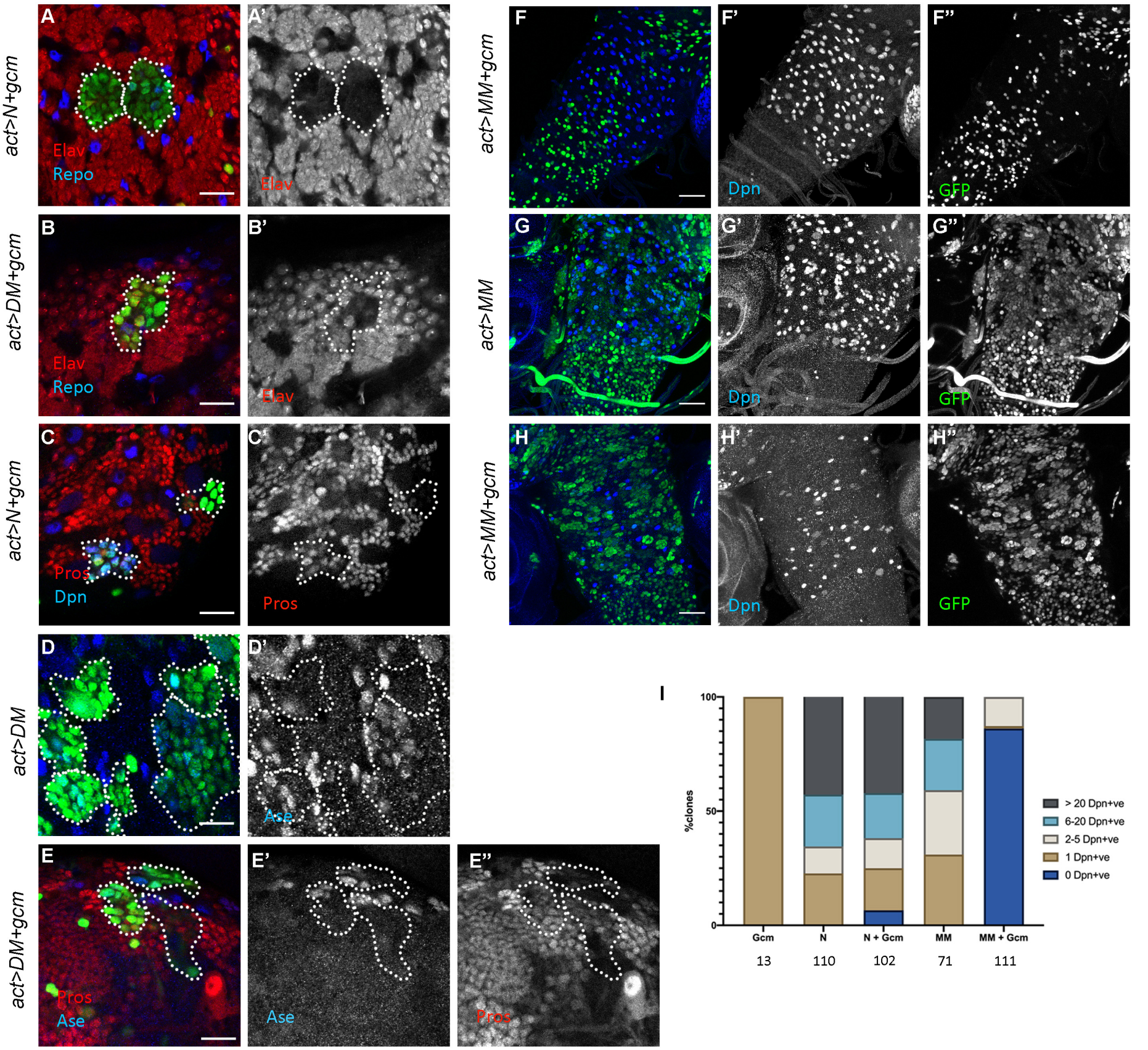

Figure S17 Effect of *gcm* misexpression on *N*, *DM* and *MM* lineages. (A-E) *act>STOP>Gal4* FLPout brain lobe clones are marked by GFP (green) and traced with dotted outlines. (A,C) misexpression of *NΔecd+gcm*. (B,E) misexpression of *DM+gcm*, (D) misexpression of *DM* (control for E). (F-H) Effect of *gcm* on the induction of Dpn (blue) by MM; entire VNCs are shown. F has no lineage clones (so the NSC number is not affected), whereas G and H have a large number of clones (see GFP-only channel in F"-H"). (I) Clones of the indicated genotypes were scored for the number of NSCs per clone. The total number of Type I clones scored for each genotype is shown below the chart. Scalebars: A-E 25µm, F-H 50µm.